Supplementary Information

for

Efficient Removal of Toxic Dyes via Simultaneous Adsorption and Solar Light Driven Photodegradation Using Recyclable Functionalized Amylopectin-TiO_2-Au Nanocomposite

Amit Kumar Sarkar[†], *Arka Saha*[⊥], *Abhrojyoti Tarafder*[‡], *Asit Baran Panda*[⊥*], *Sagar Pal* [†*]

[†] Polymer Chemistry Laboratory, Department of Applied Chemistry, Indian School of Mines, Dhanbad – 826004, India

[‡] Department of Environmental Science & Engineering, Indian School of Mines, Dhanbad – 826004, India

[⊥] Discipline of Inorganic Materials and Catalysis, Central salt and Marine Chemicals Research Institute (CSIR), Bhavnagar-364002, Gujarat, India.

[†*] Corresponding author:

Tel: +91-326-2235769; E-mail: sagarpal1@hotmail.com; pal.s.ac@ismdhanbad.ac.in (S. Pal)

[⊥*]Corresponding Author:

Tel: +91-278-2567760, Ext-704; E-mail: abpanda@csmcri.org (A. B. Panda)

Synthesis:

Synthesis of g-AP-pAA. Amylopectin (AP) was functionalized by grafting of flexible longer *poly* (acrylic acid) chains on AP backbone to obtain a copolymer with very high molecular weight and the corresponding grafting was performed following our previously reported method with some modifications.

Preparation of g-AP-pAA/TiO_2 nanocomposite. After formation of the copolymer g-AP-pAA, it was immersed in 0.1 (N) NaOH for 12 h and subsequently it was washed with methanol-water (70:30) followed by acetone to obtain pure anionic copolymer. Then the product was completely dried in a vacuum oven. Afterwards, powder g-AP-pAA was added to aqueous media, with pH 9, at a temperature of 50 °C (pH was adjusted by adding 0.1 M of NaOH) with constant stirring to get a homogeneous gelling matrix of g-AP-pAA. For optimization, pH of the suspension was varied by adding the NaOH solution (Table S1, Supporting Information). Then, 10 mL clear dry ethanoic mixture Ti-^{i}Pr was added to homogeneous gelling matrix of g-AP-pAA drop wise under vigorous stirring and the transparent gelling matrix changed to milky white. Amount of TiO_2 in the composite was varied by varying the amount of Ti-^{i}Pr in ethanoic solution (Table S1, Supporting Information). The stirring was continued for 6 h to complete the hydrolysis and polycondensation reactions. After completion of the reaction, the

milky white solution was cooled to room temperature, precipitated in acetone and placed under vacuum oven at 50°C for 24 h.

Preparation of g-AP-pAA/TiO_2-Au nanocomposite. For the synthesis of g-AP-pAA/TiO_2-Au nanocomposite, to the resultant milky white suspension formed during the synthesis of g-AP-pAA/TiO_2 after addition of Ti-^{i}Pr and 6 h of stirring, clear ethanolic solution of $HAuCl_4$ was added in dark condition at 50 °C. The wt% of Au was varied with respect to g-AP-pAA/TiO_2 (Table S1, Supporting Information). The stirring was continued up to another 12 h. The color of the reaction mixture was changed from milky white to distinct violet, confirming the *in-situ* reduction of Au^{3+} to metallic Au^0 (Au NPs). After that the mixture was precipitated in acetone and placed in vacuum oven at 50°C for 24 h.

Characterization.

The powder x-ray diffraction pattern of the composites were recorded using Bruker DAVINCI D8 ADVANCE diffractometer equipped with Cu Kα radiation, λ 0.15406 nm, with scanning range from 10° to 80°. FTIR spectral analyses were carried out using a FTIR spectrometer (Perkin Elmer, Model Spectrum 2000). The surface morphology, elemental mapping, EDX spectra of the synthesized photocatalyst was investigated by field emission scanning electron microscopy (FESEM Supra 55, Make-Zeiss, Germany). Transmission Electron Microscope (JEOL, JEM 2100 microscope) was used to determine the surface microstructure. Surface topographic images were taken using atomic force microscopy (AFM, Dimension Icon Multimode 5, Bruker, Germany). Diffuse reflectance of the nanocomposites was measured by a spectrophotometer (Cary – 5000). Raman spectra were obtained using a Renishaw InVia Reflex micro Raman spectrometer with excitation of argon ion (514 nm) lasers. The spectra were collected with a resolution of 1 cm^{-1}. Specific surface area was measured using surface area analyzer (NOVA 3200e, Quantachrome, USA) at liquid nitrogen temperature 77 K. Hydrodynamic diameter and the surface potential were measured using zeta sizer Nano ZS (Malvern, UK). Photoluminescence spectra were recorded using Perkin Elmer LS 55 Fluorescence Spectrometer.

ADSORPTION EXPERIMENT:

Removal of dyes:

A 1000 mg L^{-1} of each (MV/AO) stock solutions were prepared and diluted to required concentration for experimental conditions. For every analysis fixed quantity of adsorbent was mixed with 25 mL of dye solution in a 150 mL conical flask. pH was adjusted with addition of 0.1(N) HCl or 0.1(N) NaOH solutions. The adsorption study was conducted in orbital shaker (Make: Remi, India) under dark condition. After completion, solutions were withdrawn with fixed time interval followed by centrifugation at 10000 rpm for 10 min (Centrifuge, Make: REMI; Model-R-24). Subsequently, the concentration of dye solution was measured by UV- visible spectrophotometer (Shimadzu, Japan).

The % of adsorption was calculated using following equation:

$$\%\, Adsorption = \frac{C_0 - C_e}{C_0} \times 100 ---------- eq.(1)$$

Additionally, the equilibrium uptake was analyzed by,

$$q_e = (C_0 - C_e) \times \frac{V}{W} ---------- eq.(2)$$

Where, q_e represents equilibrium capacity of corresponding dye on the surface of adsorbent (mg g^{-1}), C_0 represents initial dye concentration (mg L^{-1}), C_e denotes equilibrium concentration of dye solution (mg L^{-1}), V represents volume of dye

solution in L and W denotes weight of adsorbent in gm. The data represented here are the average of three readings.

Selective removal of cationic MV among the mixtures of cationic and anionic dyes:

Initially 20 ppm of anionic dye, acid orange (AO) and cationic methyl violet (MV) were taken for analysis (total volume 25 mL). Then 10 mg of nanocomposite was dispersed in the mixture and placed in orbital shaker for 5 min in dark to obtain a comparative removal of dye from the mixture.

Additionally 20 ppm of individual cationic dye (MV, SF, AR) solutions were prepared. Here in also 8 mL of each dye with 10 mg of nanocomposite were taken in 150 mL conical flask and analyzed for 5 and 15 min in dark. The residual dye concentration was measured using UV-visible spectrophotometer. For comparison, similar experiment was performed with mixture of MB and MV.

Dye removal and regeneration study through degradation:

For degradation, the composite was dispersed in the concentrated MV under optimized adsorption condition, to adsorb the maximum MV and allow the light to penetrate the adsorbent (catalyst) through solution, and then irradiate sunlight.

To find out the recyclability, 10 mg of g-AP-pAA/TiO_2-Au was dispersed in 10 ppm of MV dye solution (20 mL). Then it was placed in the direct exposure of sunlight for consecutive 80 min (under clear sky from 12 PM to respective time). Then the

photo-adsorbent was separated through centrifugation and concentration of the dye was measured with respect to maximum adsorption band. Subsequently, photoadsorbent was washed several times with acetone and distilled water and fnally dried in vacuum oven. Again the same photoadsorbent was placed in previously used ppm of MV solution and the same cycles were repeated for 5 times.

For comparison three parallel degradation experiments of pure dye solution, g-AP-pAA/TiO_2 adsorbed dye solution and g-AP-pAA/TiO_2-Au adsorbed dye solution were performed.

Analysis of Hydroxyl Radicals ($OH^{\bullet}$):

In 250 mL beaker, 100 mL aqueous solution of TA and NaOH was prepared by maintaining the actual concentration. In which 30 mg of g-AP-pAA/TiO_2-Au was suspended and stirred for 10 min. Then the total system was placed in sunlight for 240 minutes. At regular predetermined interval of time 4mL solution was taken and filtered. Then PL spectra were evaluated at 425 nm excited by 315 nm light.

Antimicrobial activity:

The synthesized nanocomposites were found to be insoluble in water. Thus, to determine the antimicrobial activity, the nanocomposite was suspended in aqueous nutritional broth [R-2A Broth, formulated as Casein acid hydrolysate 0.500 g/L, Yeast extract 0.500 g/L, Proteose peptone 0.500 g/L, Dextrose 0.500 g/L, Starch (soluble) 0.500 g/L, Dipotassium phosphate 0.300 g/L, Magnesium sulphate 0.024

g/L, Sodium pyruvate 0.300 g/L, Final pH (at 25°C) 7.2±0.2], where *Escherichia coli* (gram-negative) strain was present which would be in contact with the nanocomposite. The primary stock *E. coli* strain was grown in R-2A broth liquid culture (cell count 2.8 AU). Bacterial count was measured in Absorption Unit (AU) at 700 nm.[1] Initial bacterial count for the test and the control culture was 0.05 AU. Two culture flasks were prepared with R-2A broth along with two control cultures to compare the difference of specific bacterial growth. Each of the 500 mL Erlenmeyer flasks with 250 mL of liquid media was inoculated with 4 mL of stock *E. coli* culture and kept in an orbital shaking incubator (Remi India, CIS – 24 BL) at 130 rpm and at 36 °C for one day.[2] Two of the Flasks were kept under UV light exposure (350 nm, supplied by Lafit Lighting Pvt. Ltd.) with one compound g-AP-pAA/TiO_2 and another one was control. Rest of the two flasks with one containing the nanocomposite g-AP-pAA/TiO_2-Au and the other one as control were kept under visible light source (Philips, 60W Equivalent Daylight, 5000K A19 Dimmable LED). 10 mL of culture was sampled from each of the flasks repeatedly at every 4 h interval during the incubation period to obtain microbial growth profiles.[3] Each test was performed in triplicate, where bacterial counts were determined as an arithmetic mean value.

The slides were prepared by fixing the isolated strain on 1 cm^2 glass slide and dehydrated with ethanol for 5 min. Then the prepared slides were left for overnight

in desiccator. Platinum coating was given for better visibility. Afterwards, the glass slides were fixed in a sample holder for FESEM analysis.

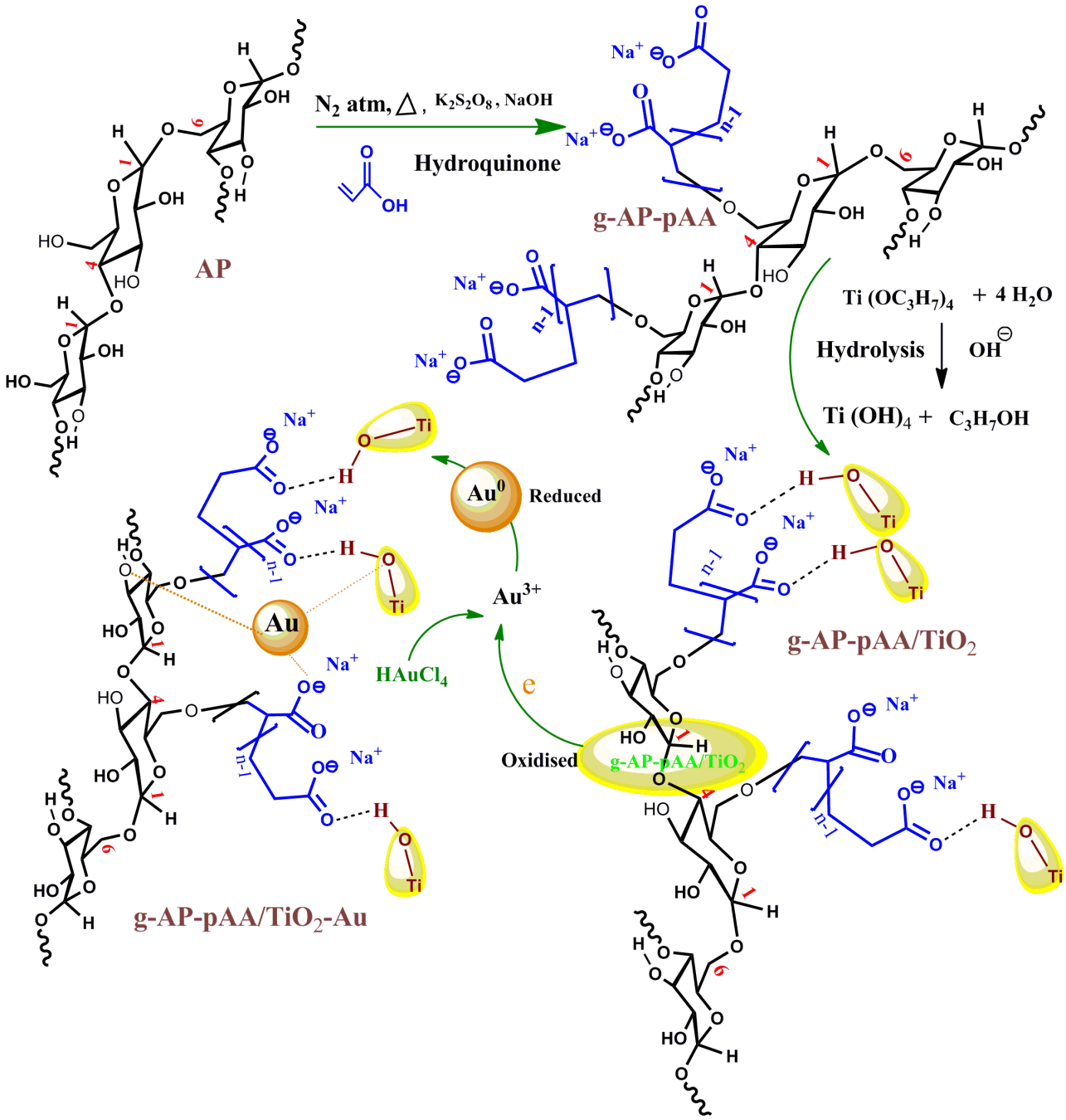

Scheme S1. Schematic representation for the synthesis of g-AP-pAA/TiO_2-Au nanocomposite

Table S1: Synthesis parameters for preparation of g-AP-pAA/TiO_2-Au nanocomposite

Nanocomposite	Amount of g-AP-pAA (Wt. %)	Amount of Ti-^{i}Pr (g)	Amount of $HAuCl_4$ (g)	pH of the reaction media
g-AP-pAA/TiO_2 1	1	2.84	-	10
g-AP-pAA/TiO_2 2	0.67	2.84	-	10
g-AP-pAA/TiO_2 3	0.67	2.84	-	9
g-AP-pAA/TiO_2 4	0.80	2.84	-	9
g-AP-pAA/$TiO_2$5	0.67	4.26	-	9
g-AP-pAA/$TiO_2$6	0.67	1.42	-	9
g-AP-pAA/TiO_2 3-Au 1	0.67	2.84	0.06	10
g-AP-pAA/TiO_2 3-Au 2	0.67	2.84	0.14	9
g-AP-pAA/TiO_2 3-Au 3	0.67	2.84	0.22	9

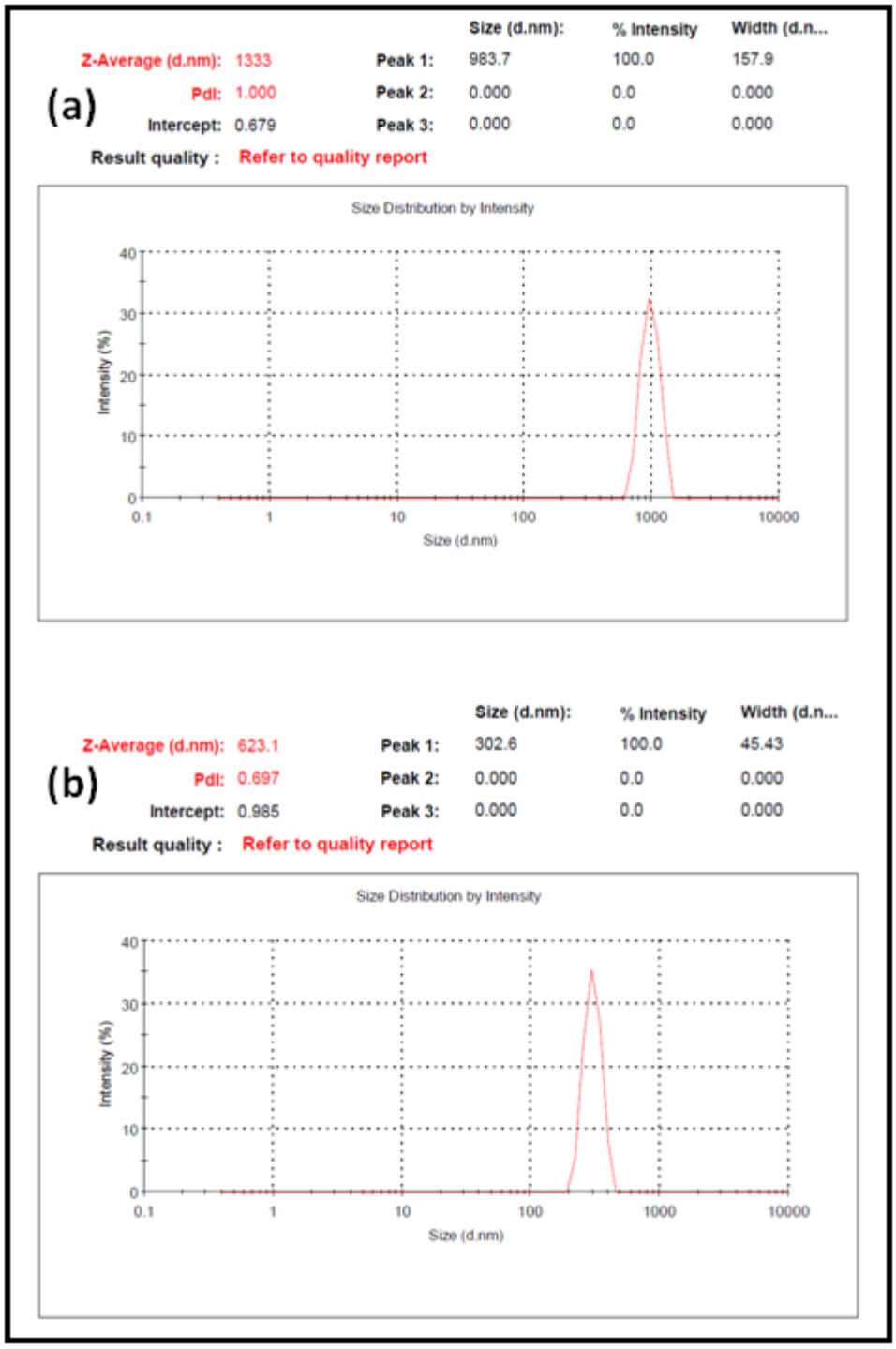

Fig. S1. Hydrodynamic diameter of g-AP-pAA (a) at pH 9 (b) at pH 7

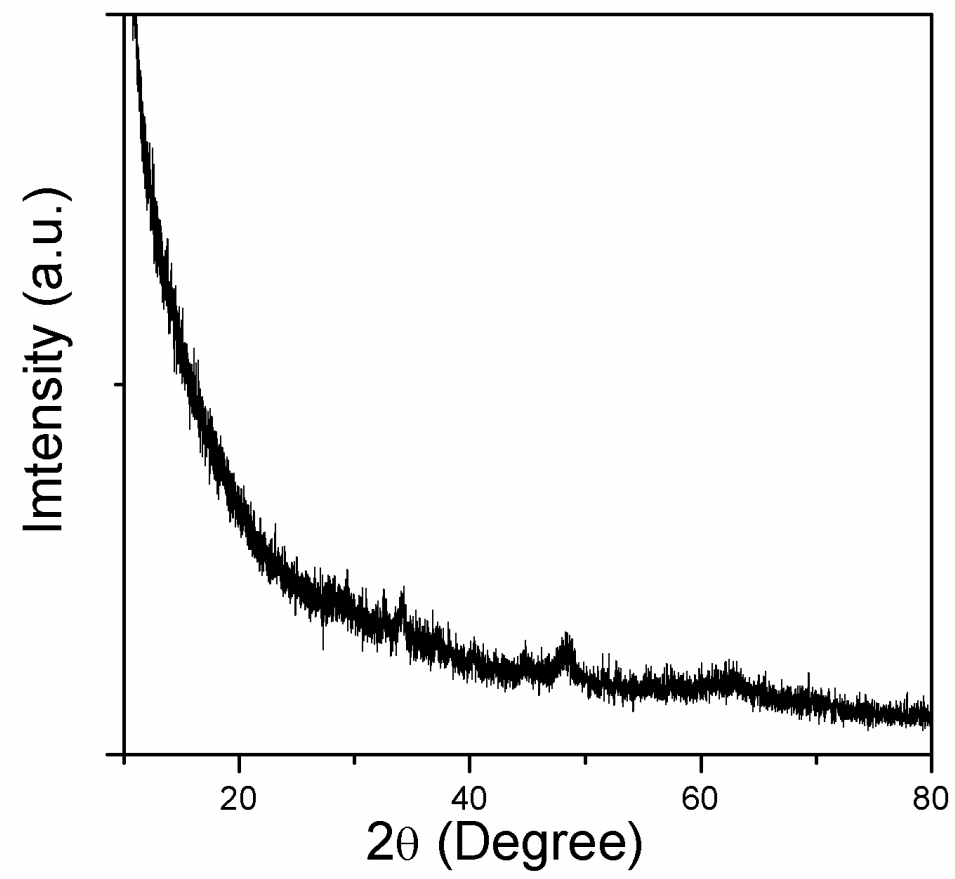

Fig. S2. XRD pattern of nanocomposite at higher pH

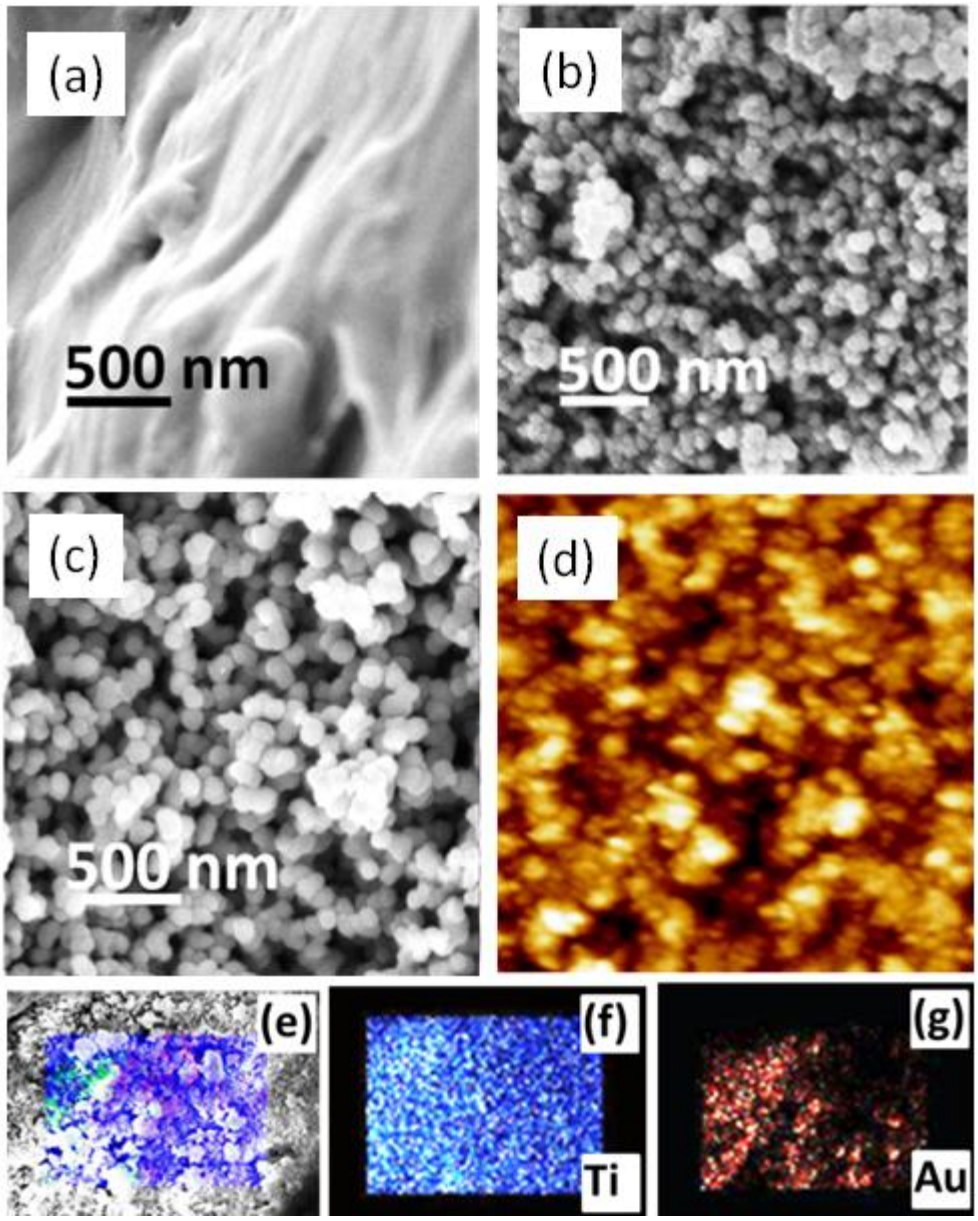

Fig. S3. FESEM images of (a) g-AP-pAA, (b) g-AP-pAA/TiO_2, (c) g-AP-pAA/TiO_2-Au, (d) AFM image of g-AP-pAA/TiO_2-Au, (e-g) elemental mapping of g-AP-pAA/TiO_2-Au

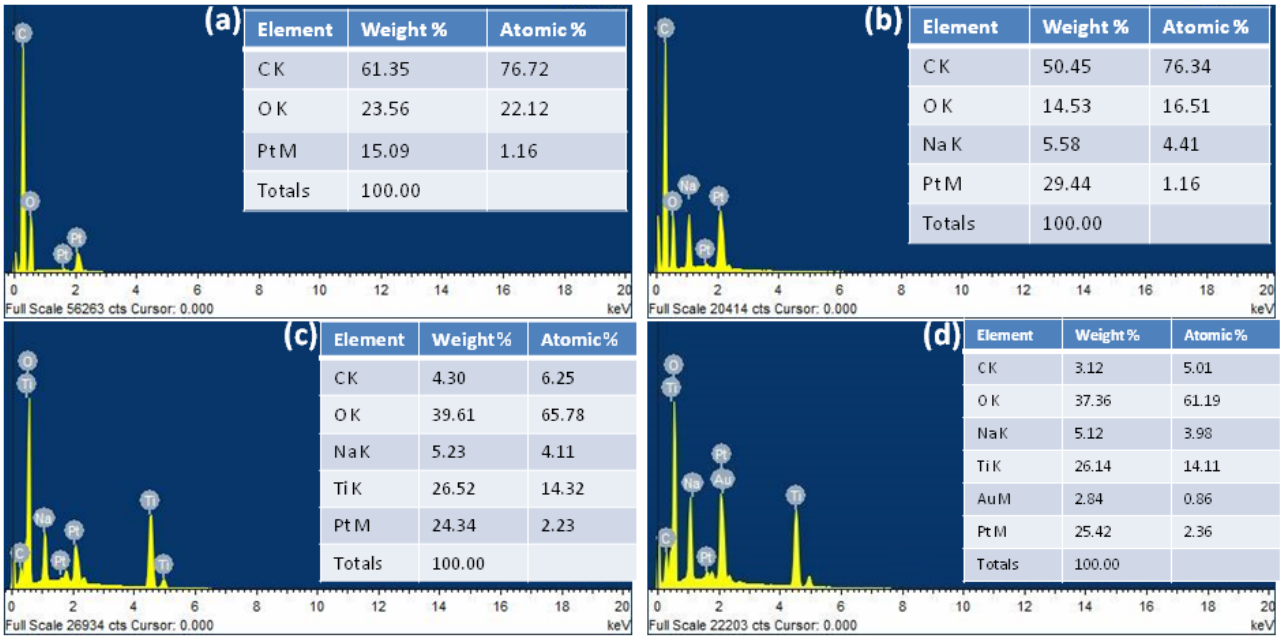

Fig. S4. EDAX analyses of (a) AP, (b) g-AP-pAA, (c) g-AP-pAA/TiO_2, (d) g-AP-pAA/TiO_2-Au nanocomposite

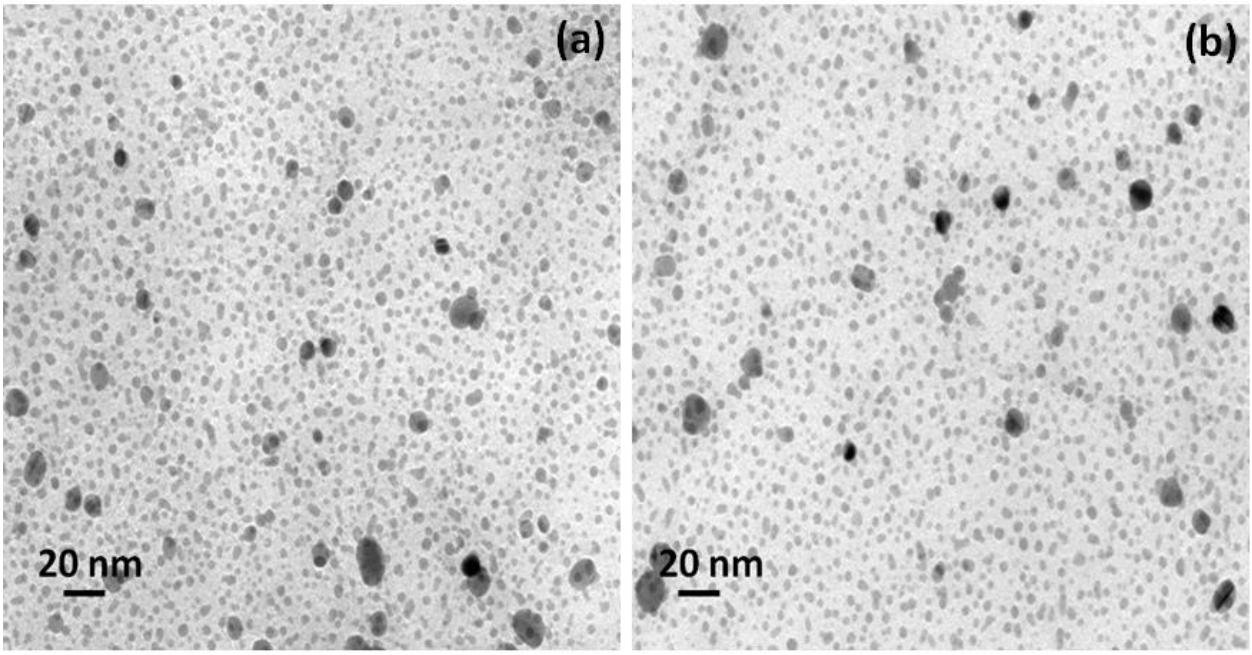

Fig. S5. TEM images of g-AP-pAA/TiO_2-Au nanocomposite

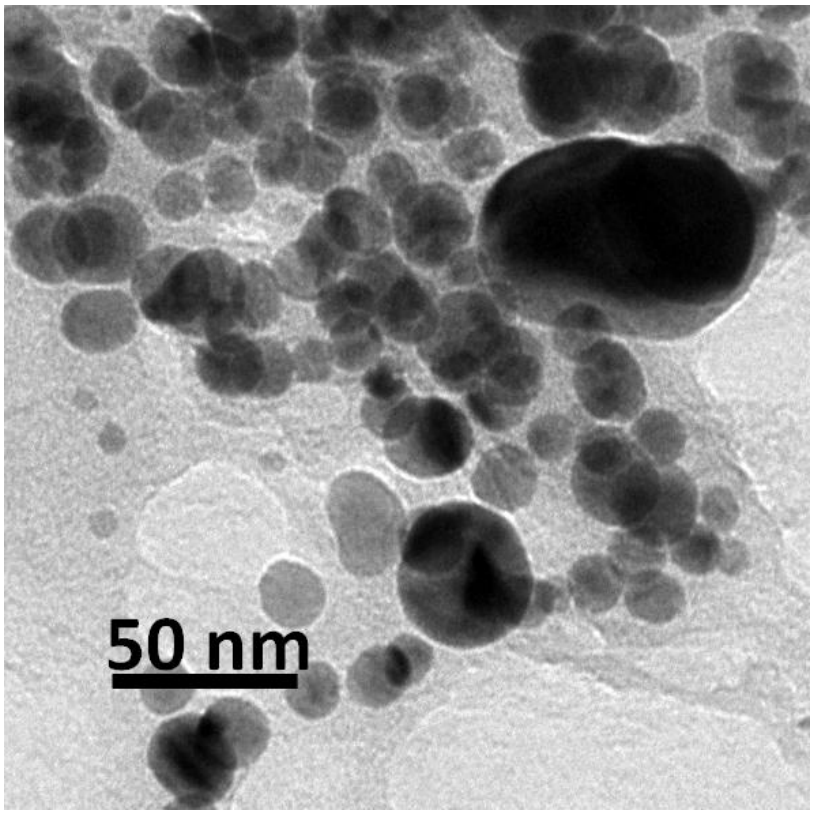

Fig. S6. TEM images of g-AP-pAA/TiO_2-Au composite with higher concentration of Au

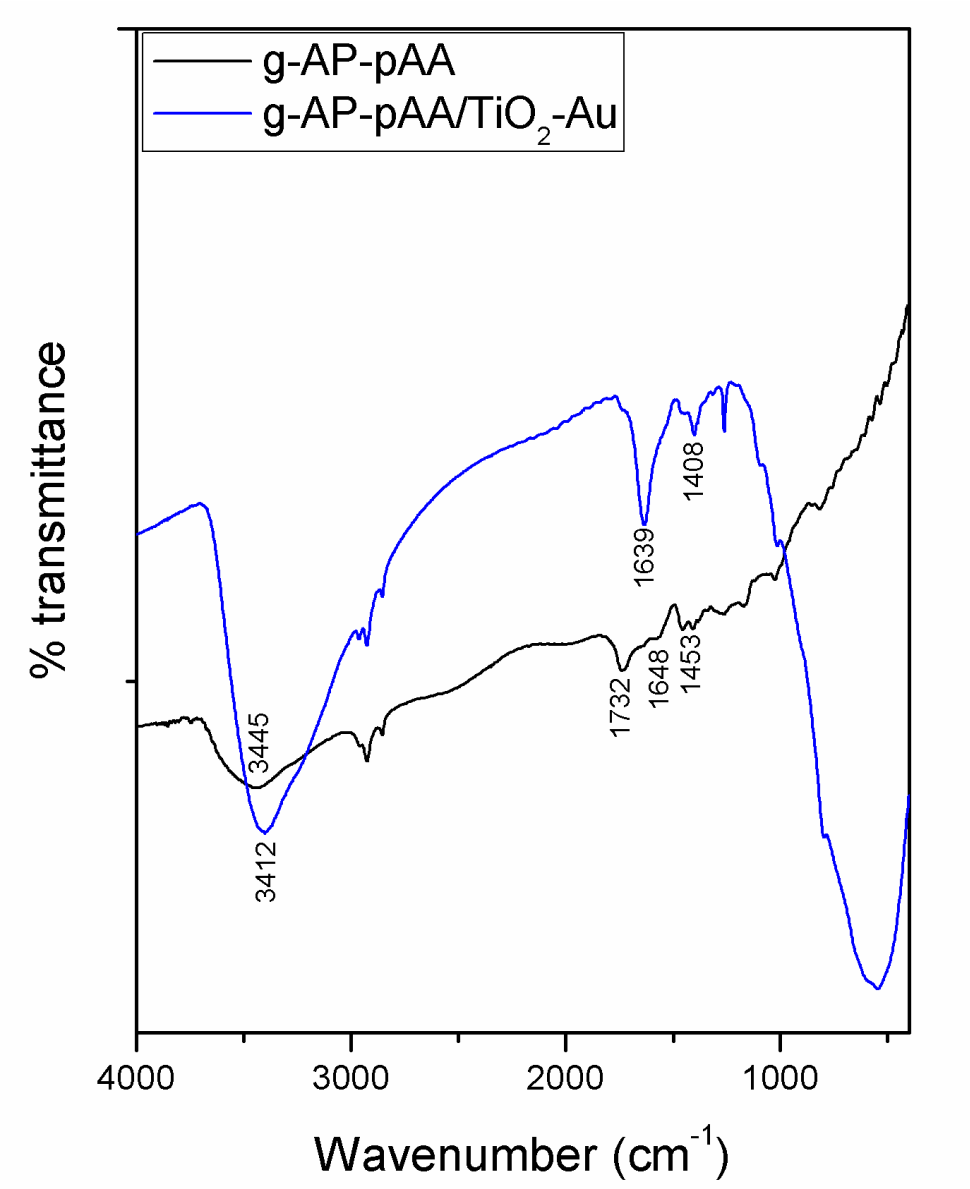

Fig. S7. FTIR spectra of g-AP-pAA and g-AP-pAA/TiO_2-Au

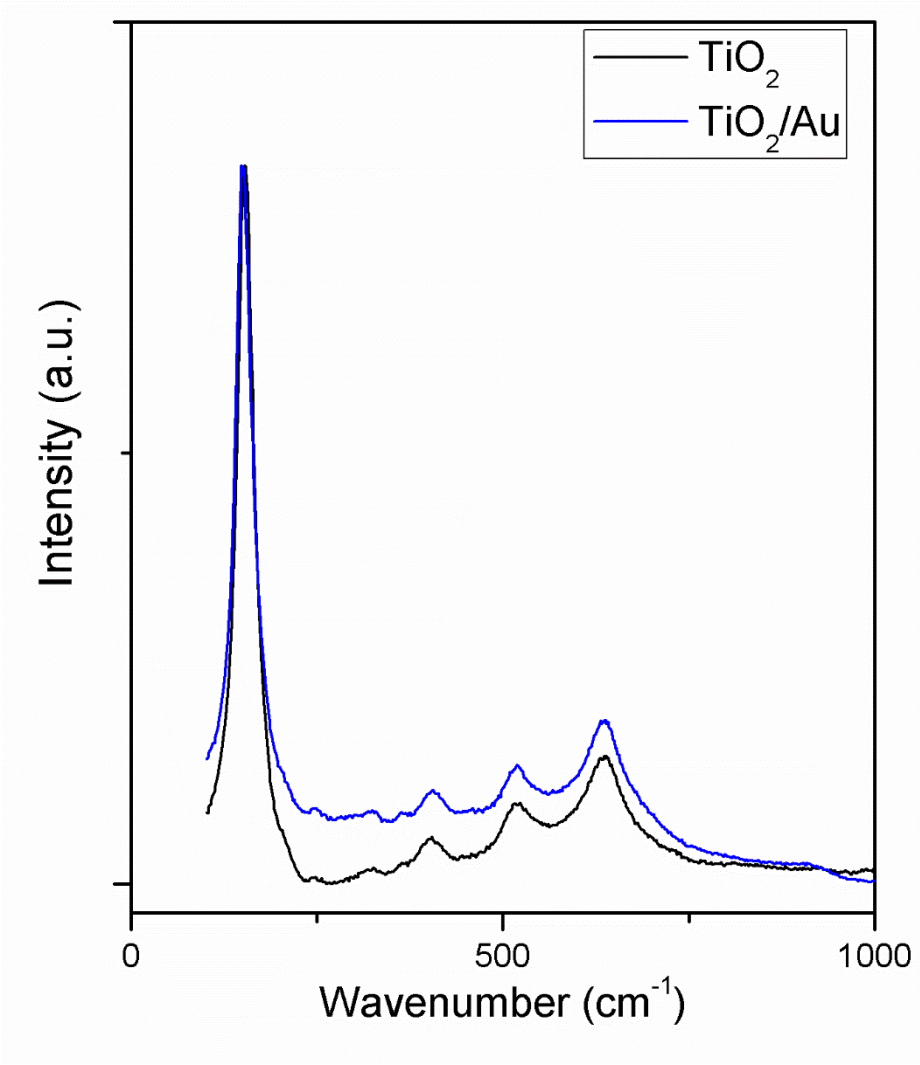

Fig. S8. Raman spectra of synthesized TiO_2 and TiO_2-Au

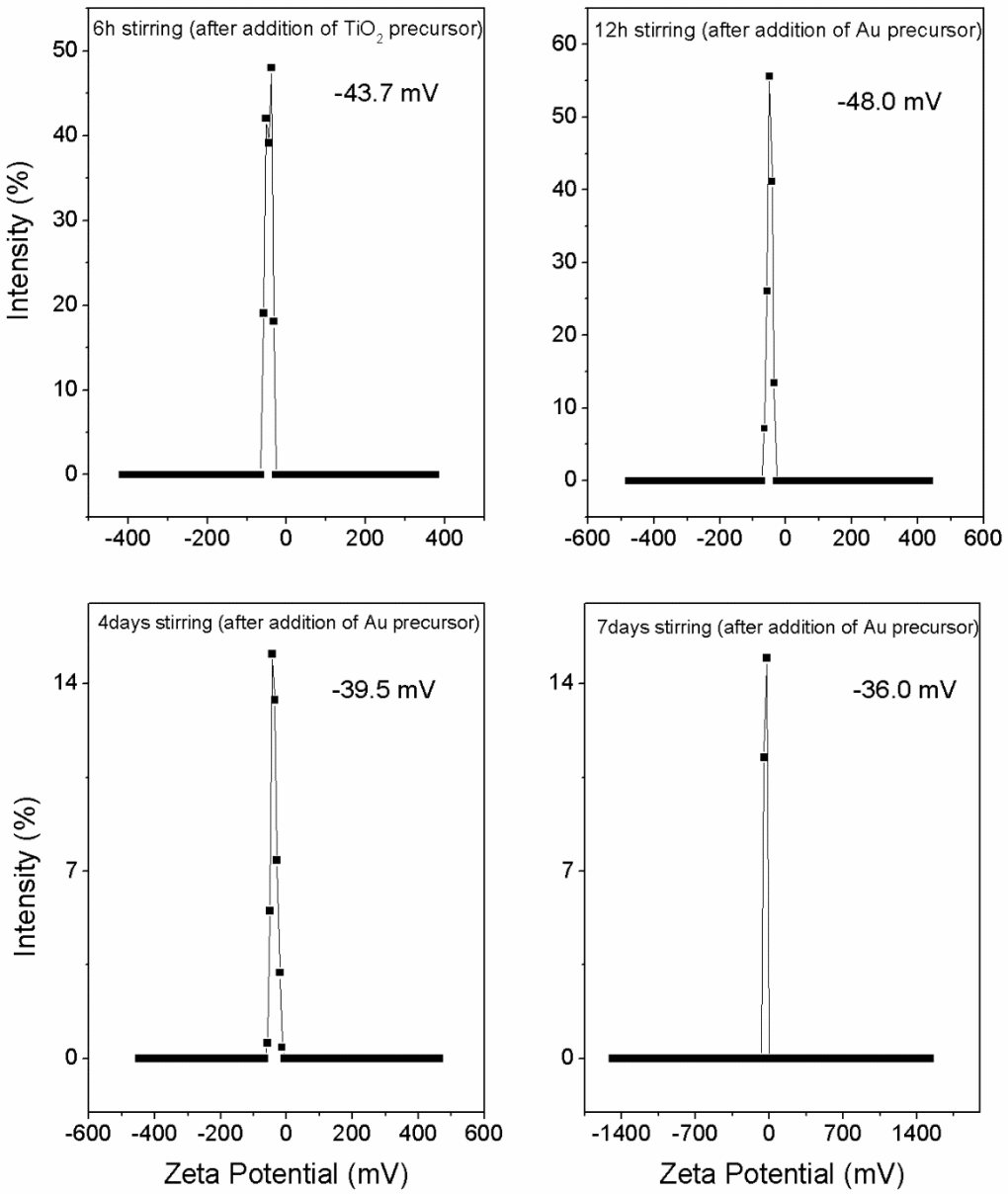

Fig. S9. Zeta potential analyses at different time intervals

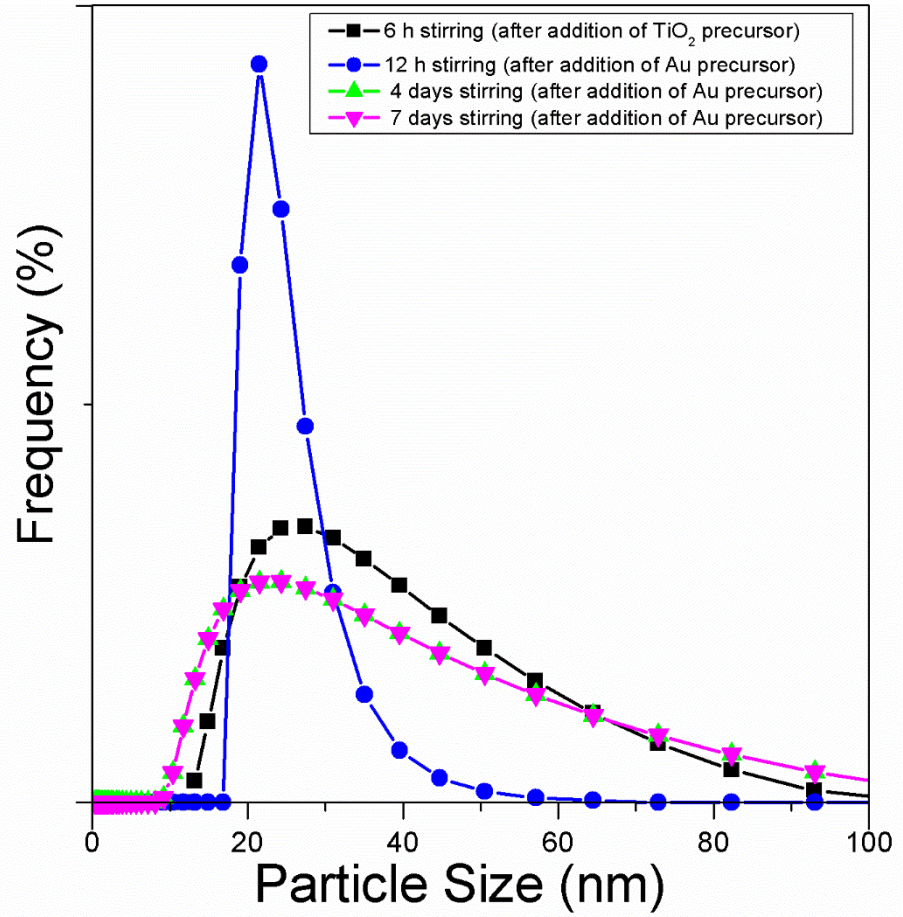

Fig. S10. DLS measurement at different time intervals

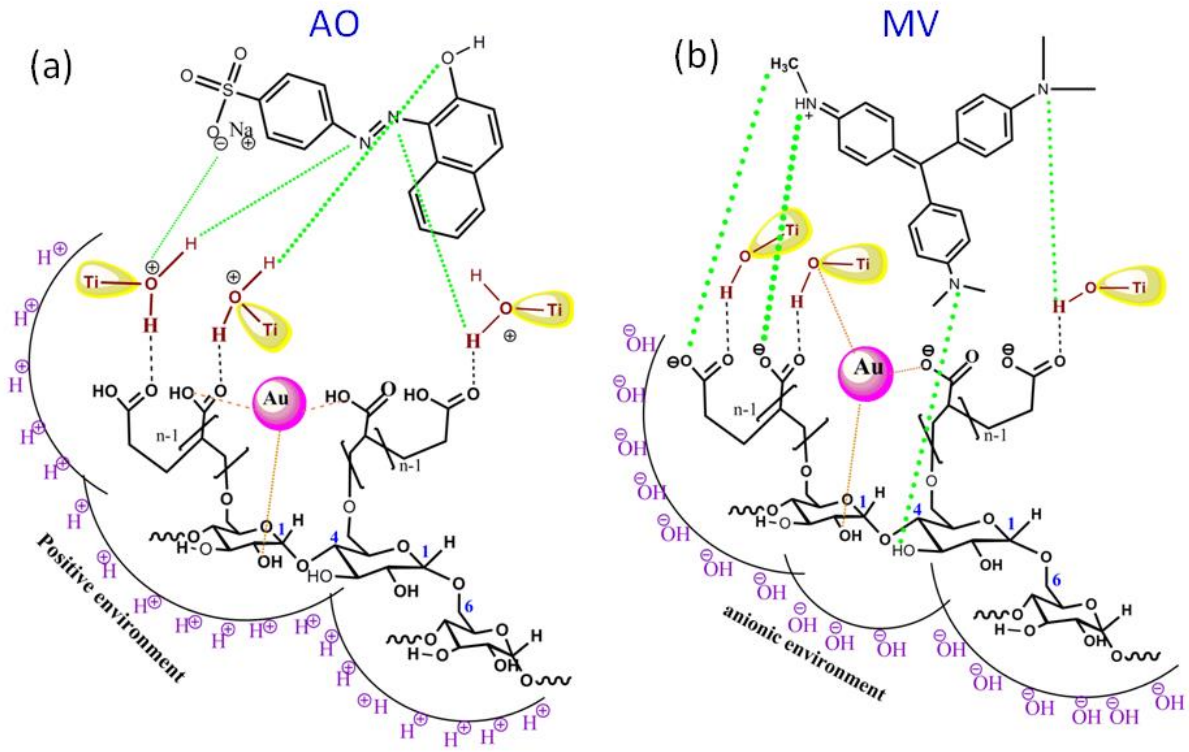

Scheme S2: Probable interaction between (a) g-AP-pAA/TiO_2-Au and AO (b) g-AP-pAA/TiO_2-Au and MV

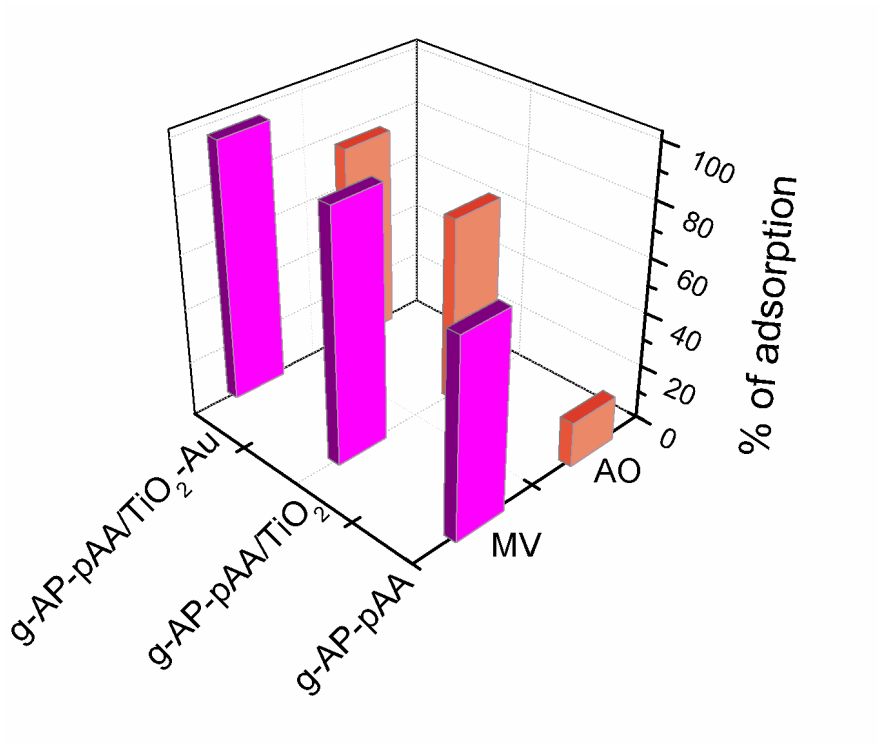

Fig. S11. Comparative adsorption characteristics of MV (pH: 8.5) and AO (pH: 4)

Table S2. Surface area of used nanocomposites

Nanocomposite	BET Surface area ($m^2 g^{-1}$)
g-AP-pAA/TiO_2	46.034
g-AP-pAA/TiO_2-Au	58.244

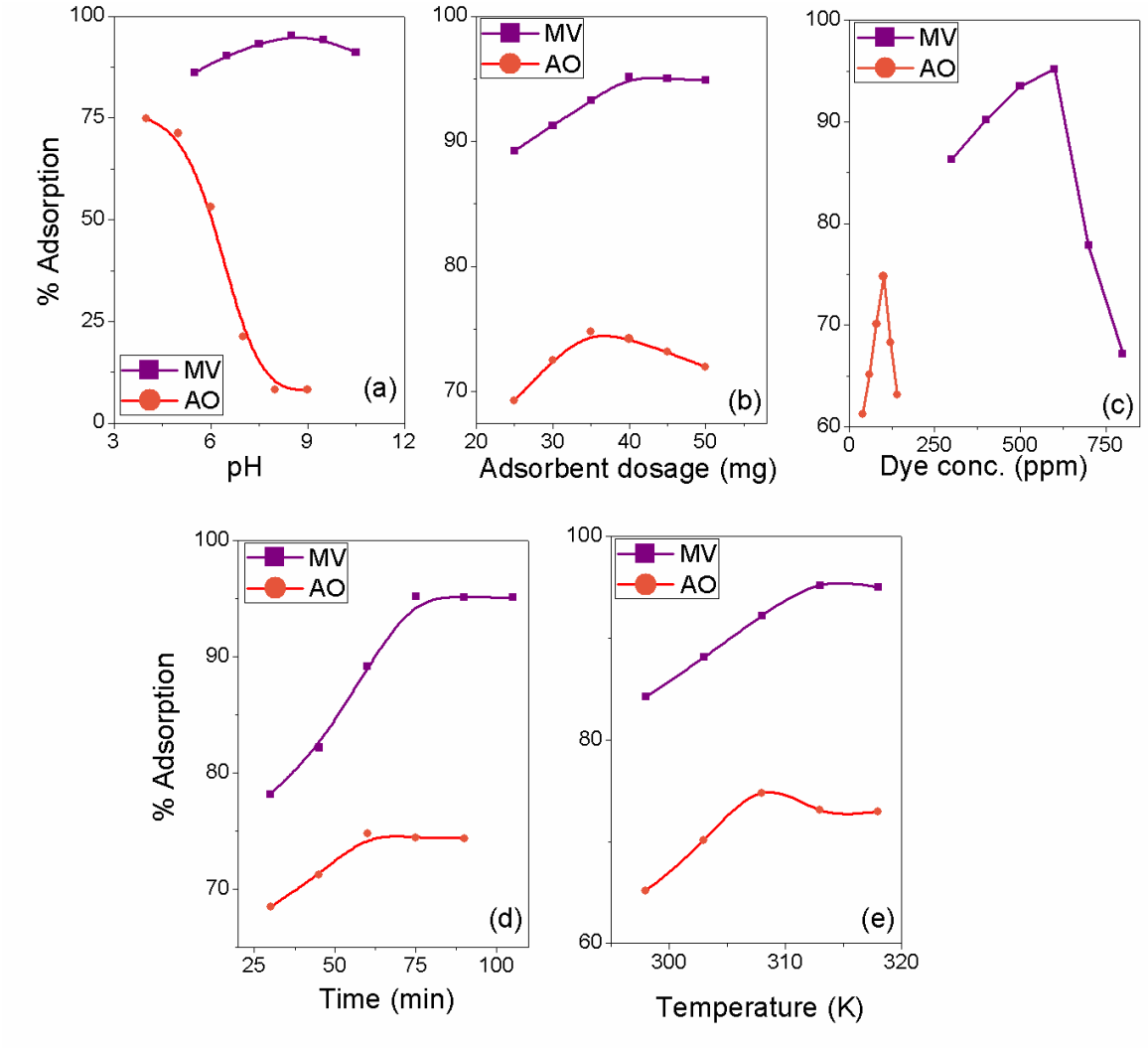

Fig. S12. (a) **pH optimization** [dosage of adsorbent: 40 mg (for MV), 35 mg (for AO); Dye conc.: 600 mg. L^{-1} (for MV), 100 mg. L^{-1} (for AO); Time: 75 min (for MV), 60 min (for AO); Temp: 313 K (MV), 308 K (AO)]**;** (b) **Adsorbent dosage optimization** [pH: 8.5 (for MV), pH: 4 (for AO); Dye conc.: 600 mg L^{-1} (for MV), 100 mg. L^{-1} (for AO); Time: 75 min (for MV), 60 min (for AO); Temp: 313 K (MV), 308 K (AO)]**;** (c) **Dye conc. optimization** [pH: 8.5 (for MV), pH: 4 (for AO); dosage: 40 mg (for MV), 35 mg (for AO); Time: 75 min (for MV), 60 min (for AO); Temp: 313 K (MV), 308 K (AO)]**;** (d) **Time Optimization [**pH: 8.5 (for MV), pH: 4 (for AO); dosage: 40 mg (for MV), 35 mg (for AO); Dye conc.: 600 mg L^{-1} (for MV), 100 mg. L^{-1} (for AO); Temp: 313 K (MV), 308 K (AO)]**;** (e) **Temperature Optimization [**pH: 8.5 (for MV), pH: 4 (for AO); dosage: 40 mg (for MV), 35 mg (for AO); Dye conc.: 600 mg L^{-1} (for MV), 100 mg. L^{-1} (for AO)]

Kinetics study:

The Legergren pseudo-first order[4] equation is expressed as:

$$\log(q_e - q_t) = \log q_e - \frac{k_1}{2.303}\, t \text{ ---------- eq(3)}$$

Where q_e and q_t (mg. g^{-1}) indicate the dye adsorbed at equilibrium and time (t) respectively and k_1 is the rate constant. Figs. S13a and S13c show the result of the plots of $\log(q_e - q_t)$ vs. t and the parameters k_1, q_e and correlation coefficient (R^2) are reported in Table S3.

The linear form of the pseudo second order kinetic rate equation[5] is represented as:

$$\frac{t}{q_t} = \frac{1}{k_2 q_e^2} + \frac{t}{q_e} \text{ ---------- eq(4)}$$

Where, k_2 (g mg^{-1} min^{-1}) is the pseudo second order rate constant. Figs. S13b and S13d demonstrate the plot of t/q_t vs. t and the parameters k_2 , q_e and R^2 values are listed in Table S3.

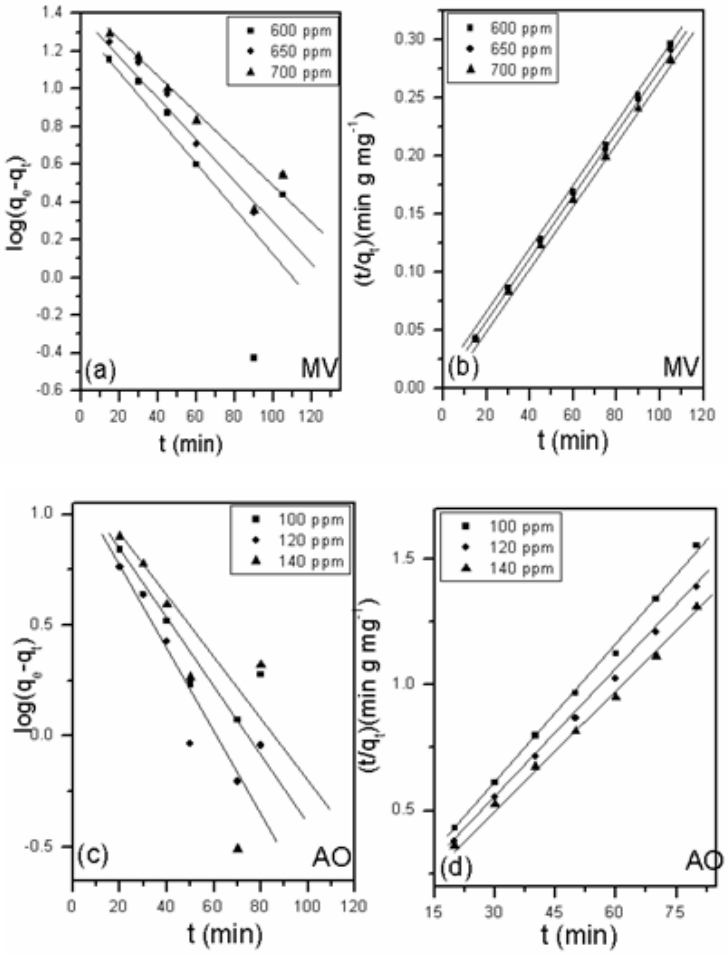

Fig. S13. Kinetics modeling of the adsorption of MV/AO onto g-AP-pAA/TiO_2-Au using (a)-(c) pseudo-first order; and (b)-(d) pseudo-second order models

Table S3: Kinetics parameters for AO and MV adsorption using g-AP-pAA/TiO_2-Au as adsorbent

Conc. (ppm)	Dye	Pseudo-first order			Pseudo-second order		
		R^2	K_1 ($g.mg^{-1}min^{-1}$)	q_e ($mg.g^{-1}$)	R^2	K_2 ($g.mg^{-1}min^{-1}$)	q_e ($mg.g^{-1}$)
100	AO	0.6892	1.83×10^{-1}	18.41	0.9981	5.25×10^{-3}	392.909
120		0.7527	1.81×10^{-1}	42.47	0.9991	4.83×10^{-3}	411.903
140		0.8241	1.71×10^{-1}	67.28	0.9992	3.12×10^{-3}	434.279
600	MV	0.5541	3.05×10^{-1}	23.752	0.9981	3.12×10^{-3}	358.422
650		0.8552	2.20×10^{-1}	23.777	0.9985	2.61×10^{-3}	366.300
700		0.8892	2.15×10^{-1}	27.644	0.9990	2.27×10^{-3}	377.358

Adsorption isotherm:

Analysis of isotherm is very significant for emphasizing the maximum adsorption capacity of adsorbent. Our present study relates the adsorption isotherm with the help of Langmuir isotherm and Freundlich isotherm models. The equation of Langmuir isotherm[6] model is,

$$\frac{c_e}{q_e} = \frac{1}{q_m b} + \frac{c_e}{q_m} ---------- \text{eq (5)}$$

Where q_e (mg.g^{-1}) denotes amount of MV adsorbed in adsorbent (per unit mass), q_m described maximum adsorption capacity, C_e (mg. L^{-1}) is the amount of dye adsorbed at equilibrium, b (L. mg^{-1}) is the Langmuir constant, relates to the affinity of binding sites. Separation or equilibrium parameter (R_L) was emphasized to find out the whether the isotherm is favorable ($0<R_L<1$) or not (RL > 1).[7]

$$R_L = \frac{1}{1 + \mathrm{b.C_0}} ----------\text{eq. (6)}$$

Where, b, C_0 represents the Langmuir constant (L. mg^{-1}) and initial dye concentration (mg. L^{-1}). The Freundlich equation[8] is,

$$lnq_e = lnK_F + \frac{1}{n_F} lnC_e ---------- \text{eq(7)}$$

K_F (mg. g^{-1}) denotes Freundlich constants related to the adsorption capacity and and n_F is the adsorption strength, respectively. q_e and C_e have same meanings, as

illustrate in Langmuir isotherm. In Freundlich isotherm n_F ($0<n_F<10$) value revealed the adsorption is favorable or not.

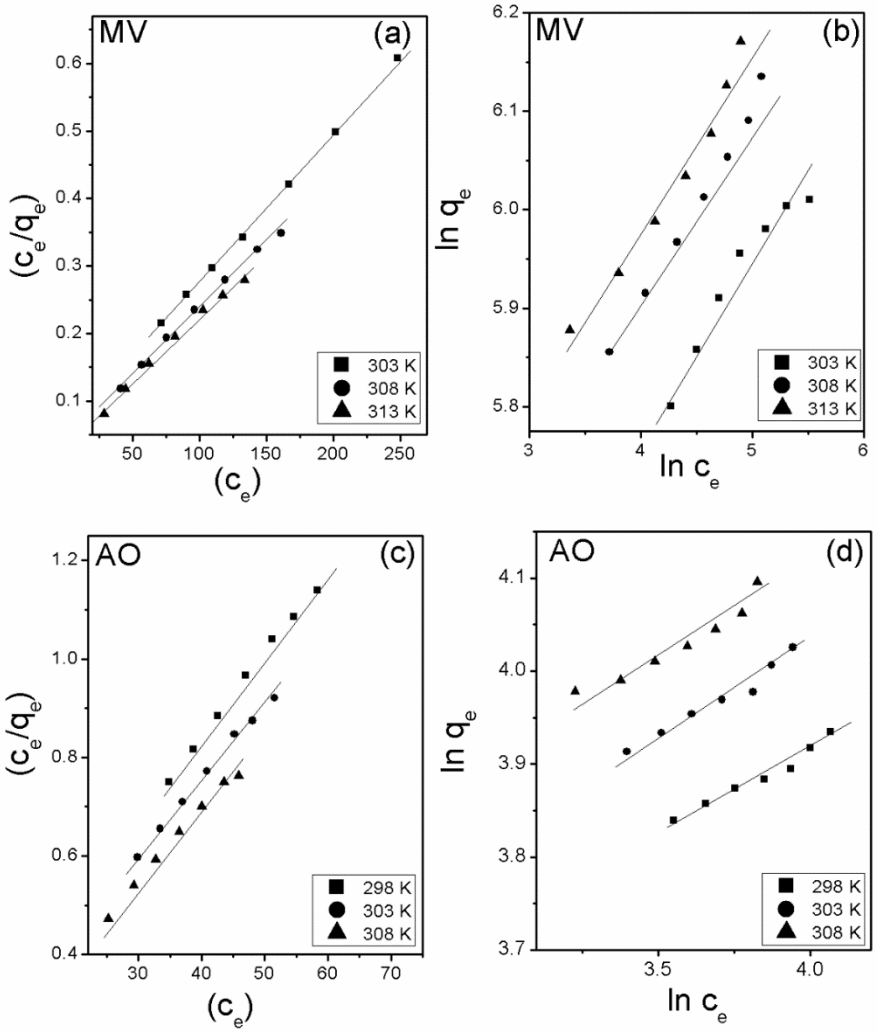

Fig. S14. Langmuir isotherm model for (a) MV and (c) AO; Freundlich isotherm model for (b) MV and (d) AO removal using g-AP-pAA/TiO_2-Au nanocomposite

Table S4: Parameters for Langmuir and Freundlich isotherm for AO/MV adsorption using g-AP-pAA/TiO_2-Au nanocomposite

Dye	Temp. (K)	Langmuir model			Freundlich model		
		Q_{max} ($mg.g^{-1}$)	b ($L.\ mg^{-1}$)	R^2	K_f ($mg.g^{-1}$)	n_f	R^2
AO	298K	51.13	0.0479	0.9940	22.87	5.424	0.9492
	303K	53.96	0.0796	0.9945	28.86	9.764	0.8940
	308K	55.65	0.0566	0.9952	32.19	9.923	0.8907
MV	303K	452.48	0.0399	0.9982	166.22	5.817	0.9266
	308K	515.46	0.0441	0.9989	165.67	5.076	0.9874
	313K	526.31	0.0566	0.9991	187.72	5.393	0.9648

Based on the R^2 values (Table S4), it can be observed that the Langmuir isotherm model demonstrated a better fit with the experimental data in comparison to the Freundlich isotherm model.

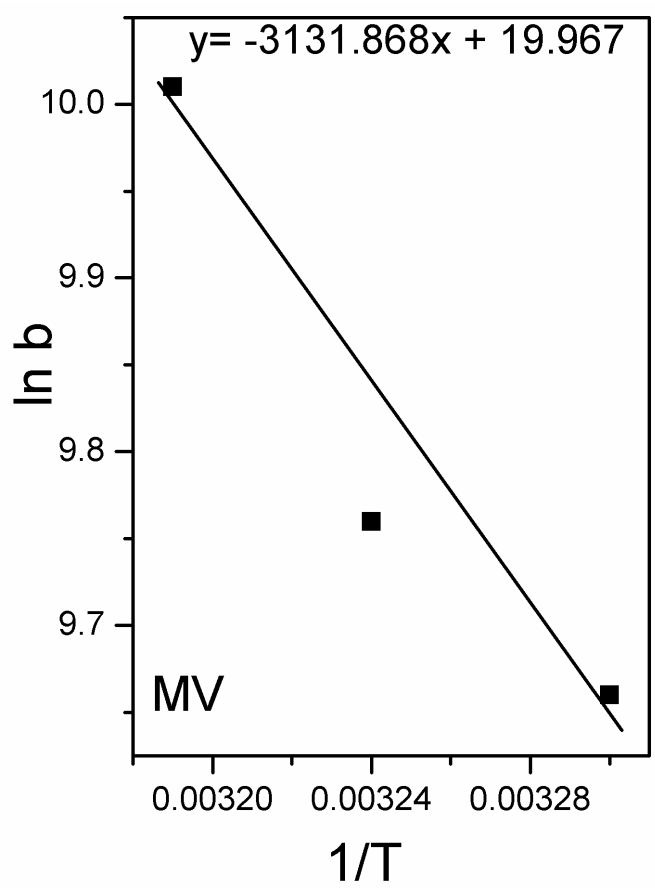

Fig. S15. Graph of ln b vs. 1/T by using g-AP-pAA/TiO_2-Au

Table S5. Thermodynamic parameters for MV using g-AP-pAA/TiO_2-Au

Temperature (K)	ΔG^0 (KJ. mol^{-1})	ΔH^0 (KJ. mol^{-1})	ΔS^0 (KJ. $mol^{-1}K^{-1}$)
303	-24.263		
308	-25.093	26.03	0.1660
313	-25.923		

Table S6. Comparative removal of adsorption capacity of MV with various reported adsorbent:

Sl. No.	Adsorbent used	Adsorption Capacity ($mg.g^{-1}$)	Degradative nature	Ref.
1.	N-benzyltriazole derivatized dextran	95.24	NO	9
2.	*Casuarina equisetifolia* needle	164.99	NO	10
3.	Cross linked amphoteric starch	333.3	NO	11
4.	h-XG/SiO_2-2	378.8	NO	12
5.	Halloysite nanotubes	113.6	NO	13
6.	natural peach gum	277	NO	14
7.	Granular activated carbon	95	NO	15
8.	**g-AP-pAA/TiO_2-Au**	**526.31**	**YES**	**Present study**

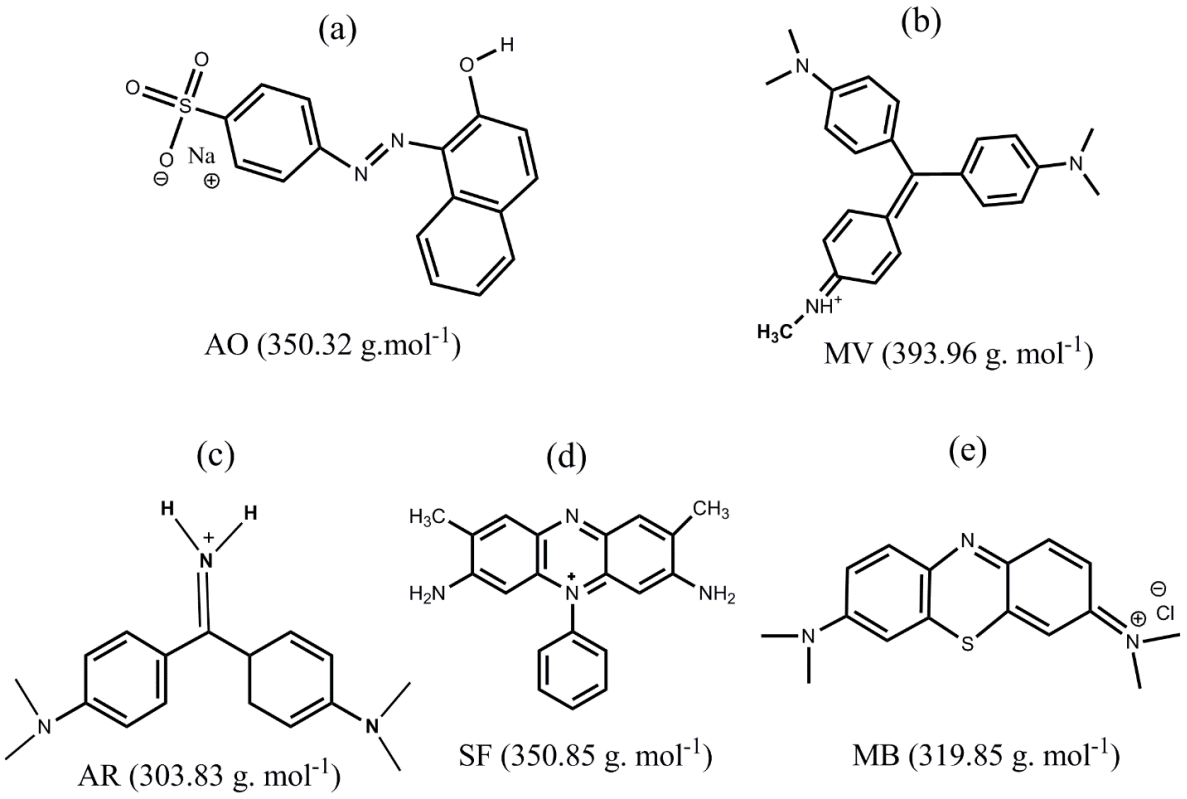

Fig. S16. Structural presentation and molecular weight of various cationic and anionic dyes used

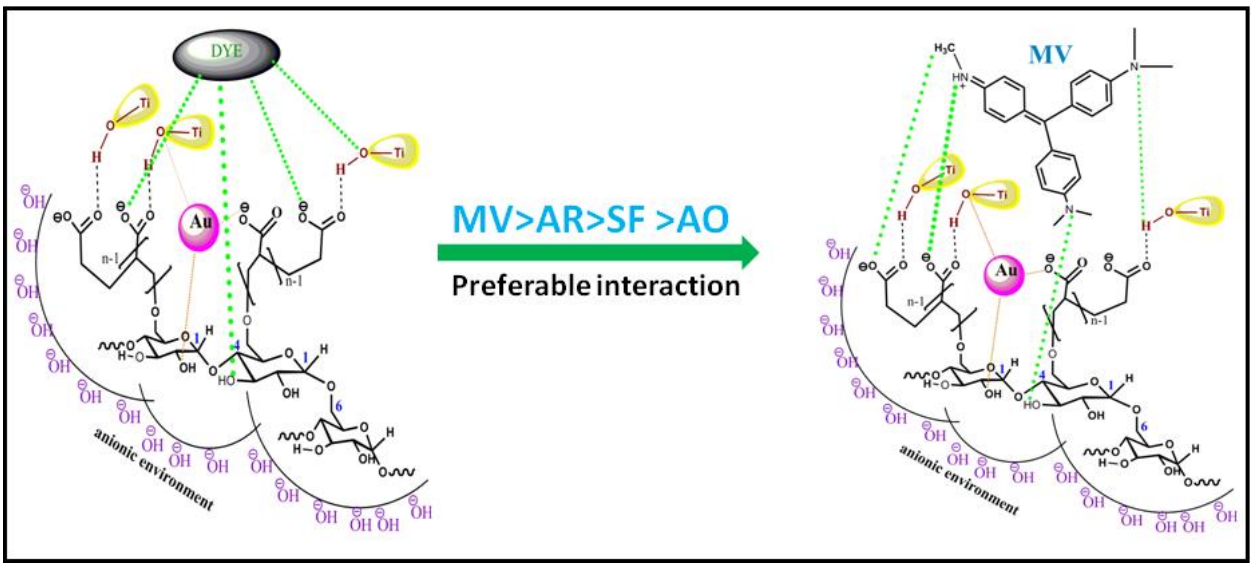

Scheme S3. Preferable interaction between different cationic dyes with g-AP-pAA/TiO_2-Au nanocomposite

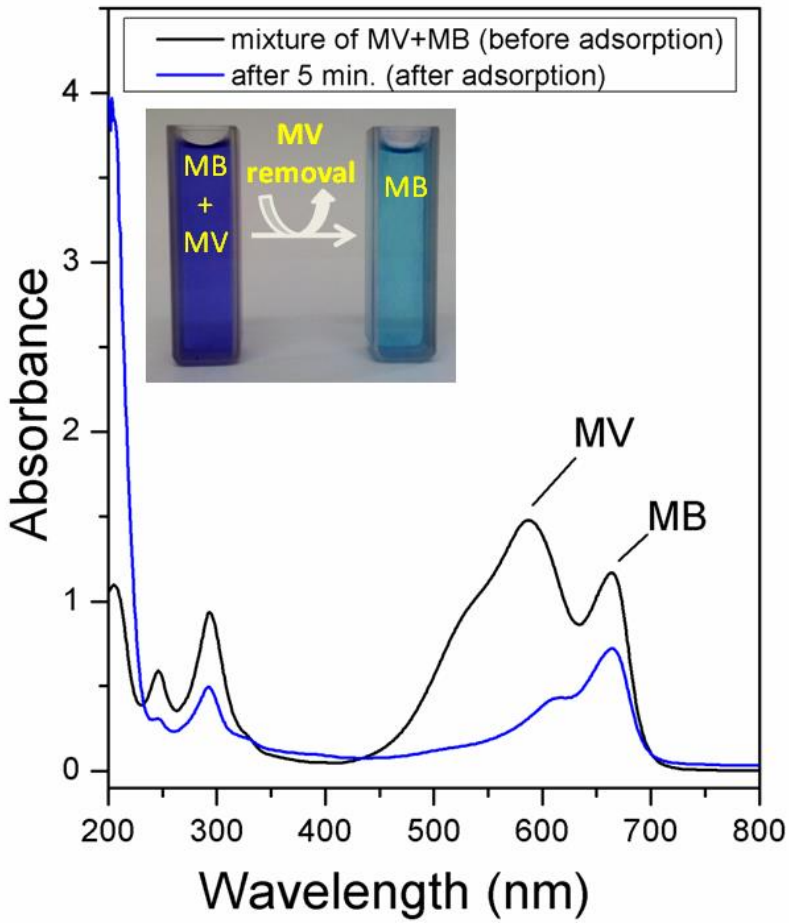

Fig. S17. Selective removal of MV from mixtures of MV and MB

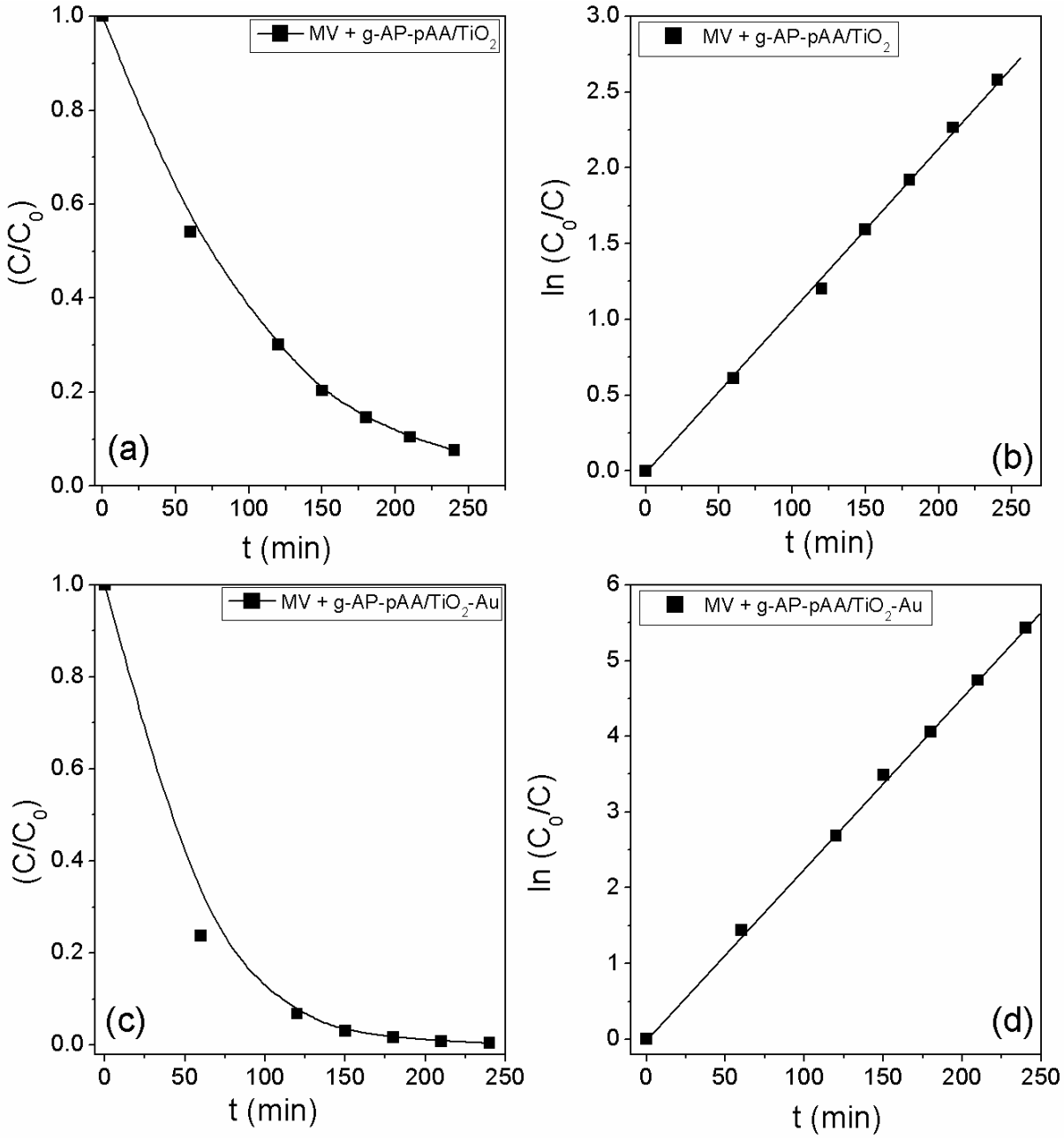

Fig. S18. Performances of nanocomposites for photocatalytic degradation of MV in presence of sunlight

Table S8: Rate constant for MV/AO degradation under sunlight irradiation

Photoadsorbent	Dye	Light source	k (min^{-1})
g-AP-pAA/TiO_2	MV	Sunlight	0.0108
g-AP-pAA/TiO_2-Au	MV	Sunlight	0.0224

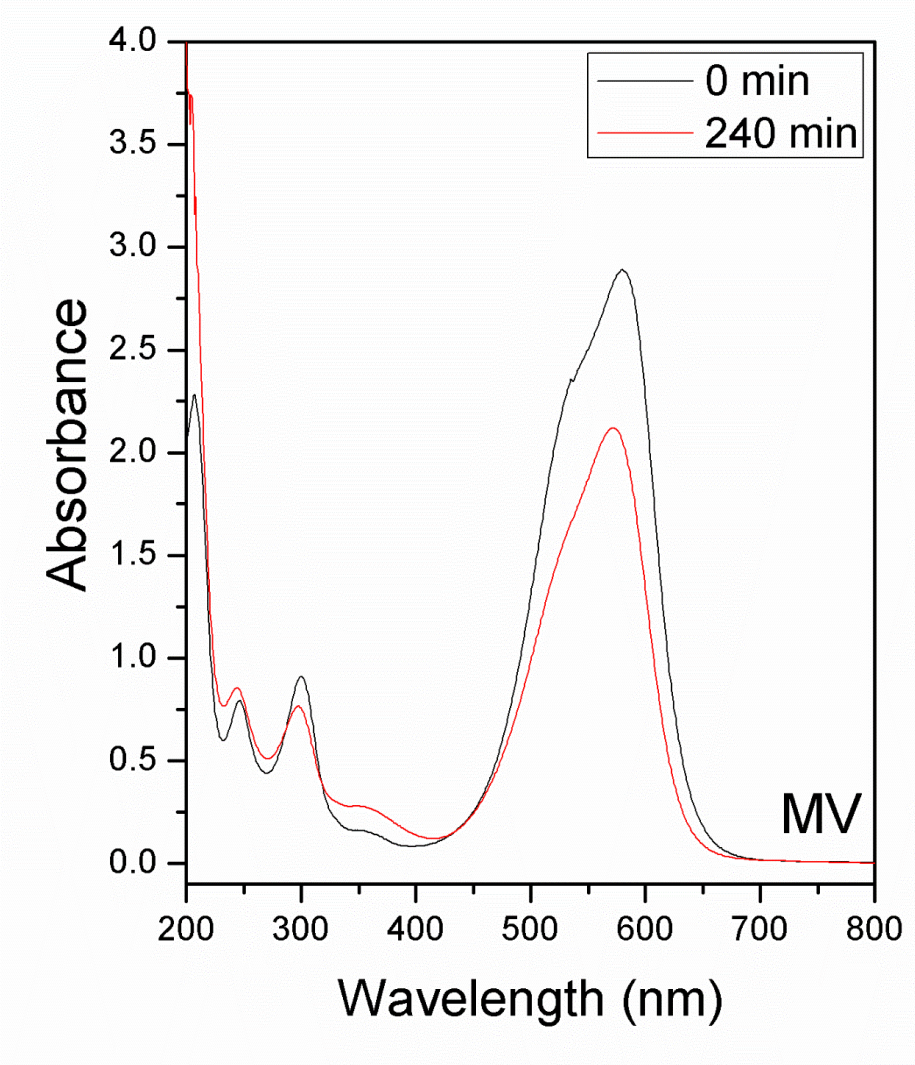

Fig. S19. Only sunlight driven degradation of MV with absence of synthesized photocatalysts

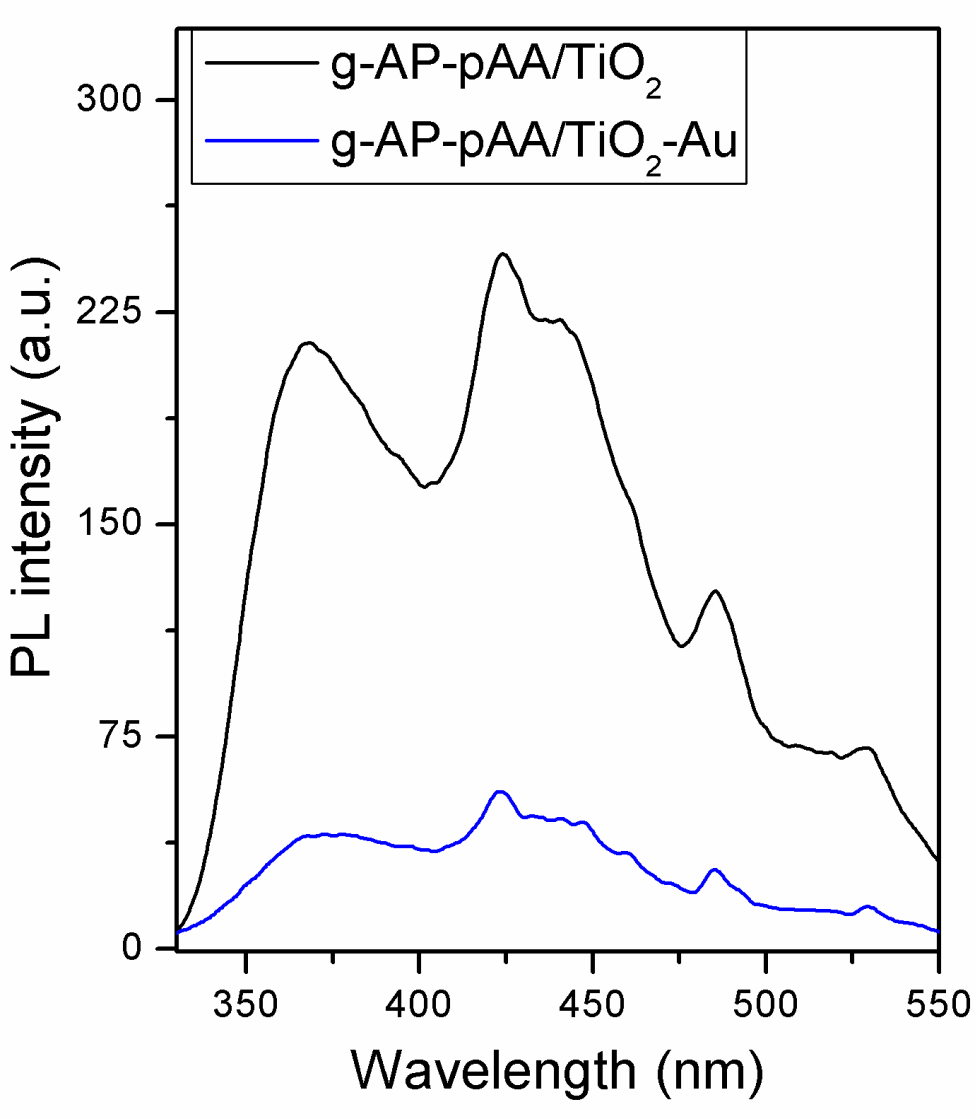

Fig. S20. PL emission spectra of photocatalysts using light of wavelength 300 nm

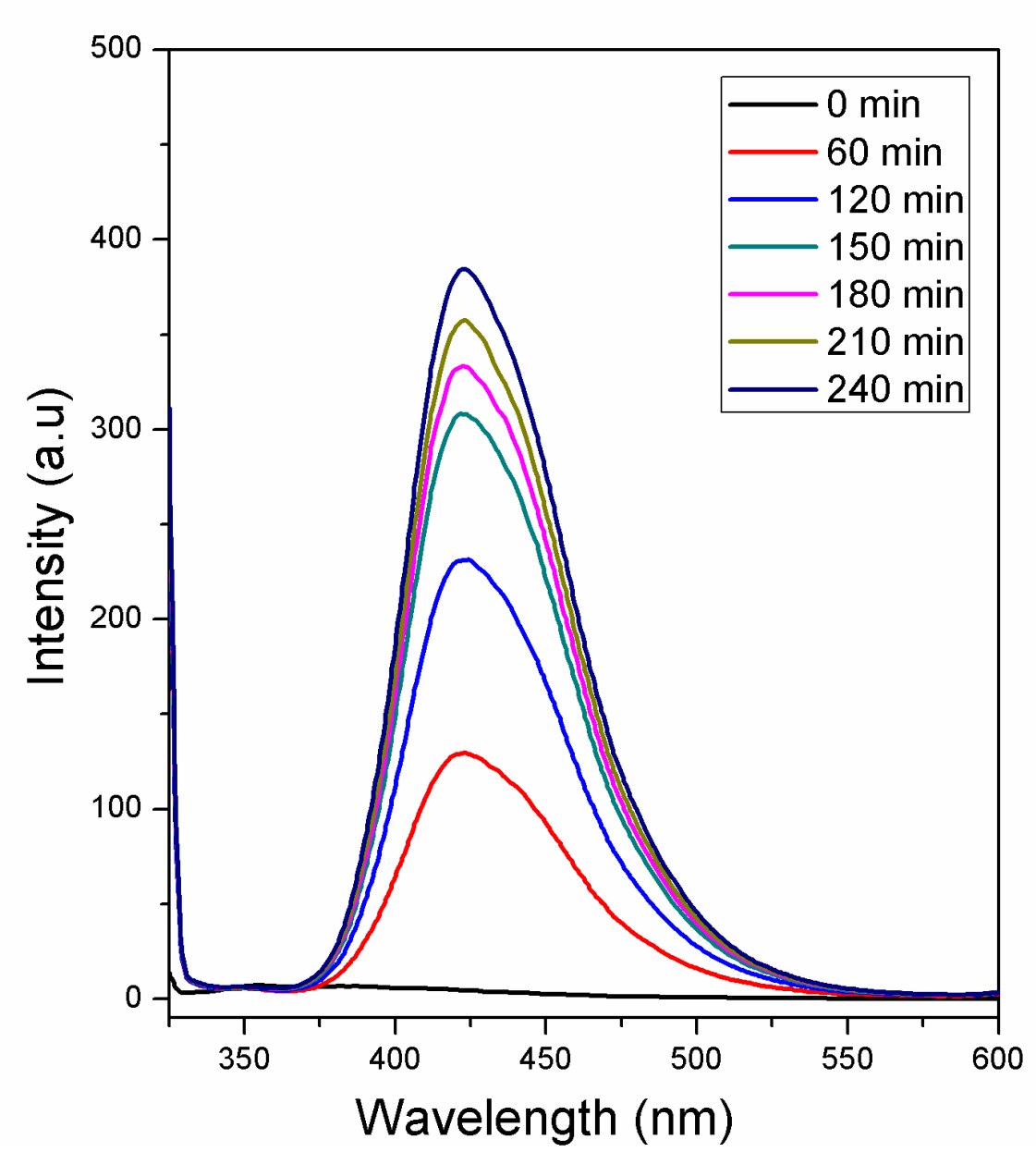

Fig. S21. PL intensity changes during OH• trapping by Terepthalic acid (TA) solution

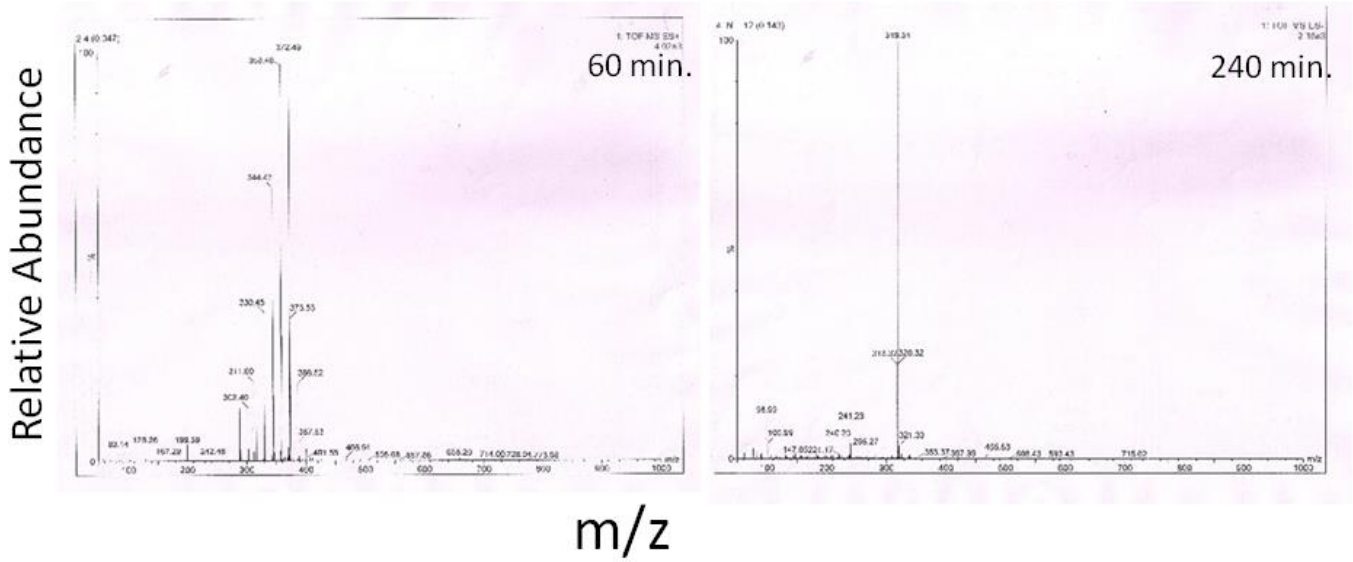

Fig. S22. N-de-methylated intermediates of MV by LC-MS technique

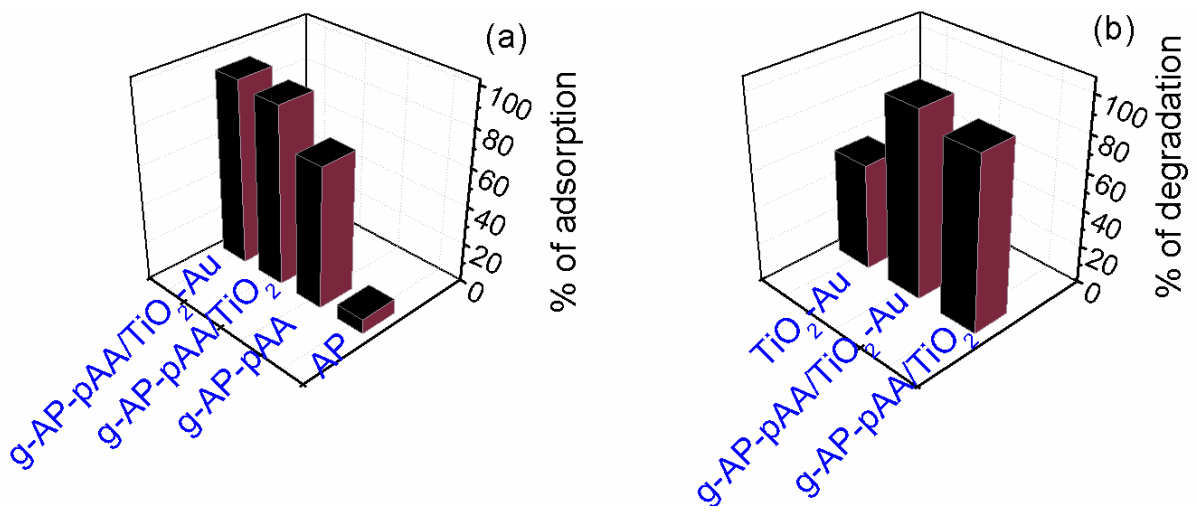

Fig. S23. (a) % dye adsorption (b) % dye degradation of nanocomposite and his individual counterparts

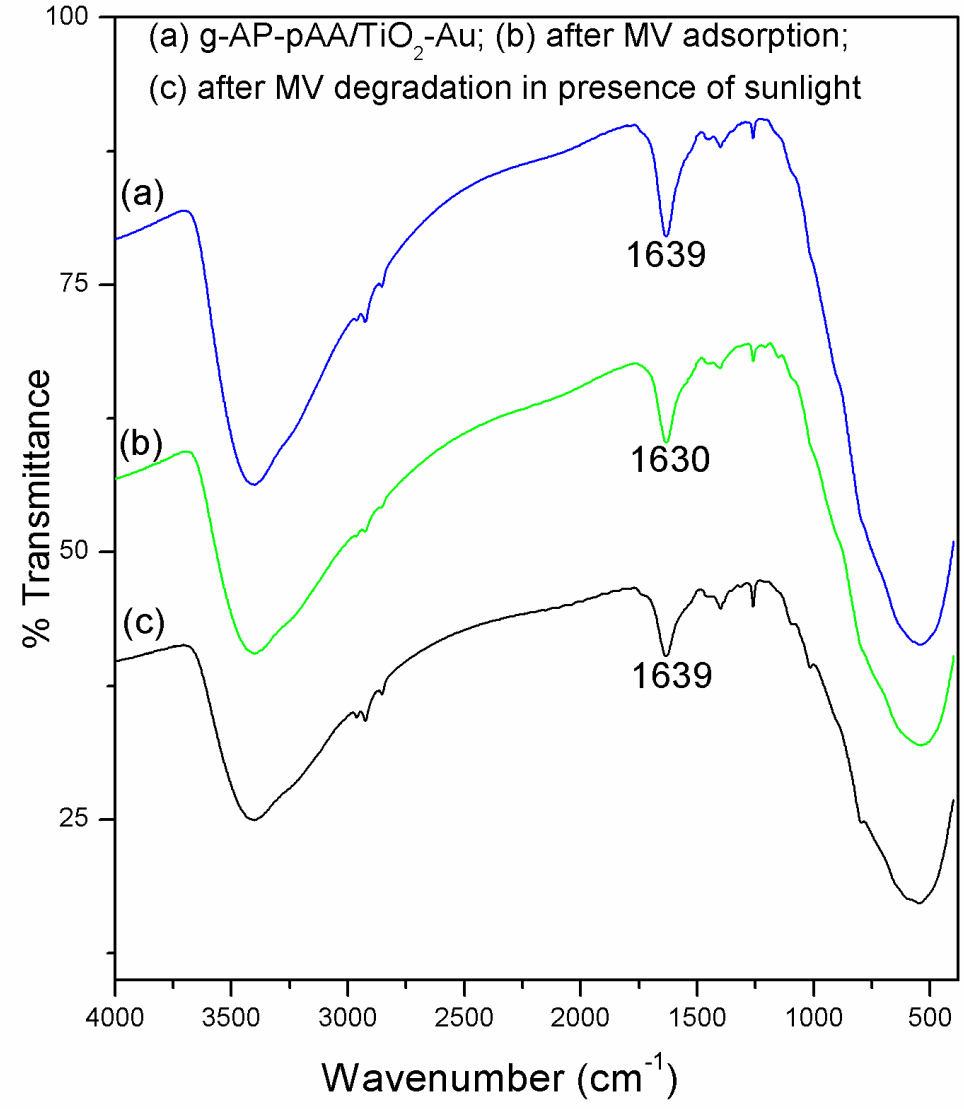

Fig. S24. FTIR spectra of (a) g-AP-pAA/TiO_2-Au nanocomposites (b) MV loaded g-AP-pAA/TiO_2-Au nanocomposites (c) MV degraded g-AP-pAA/TiO_2-Au nanocomposites

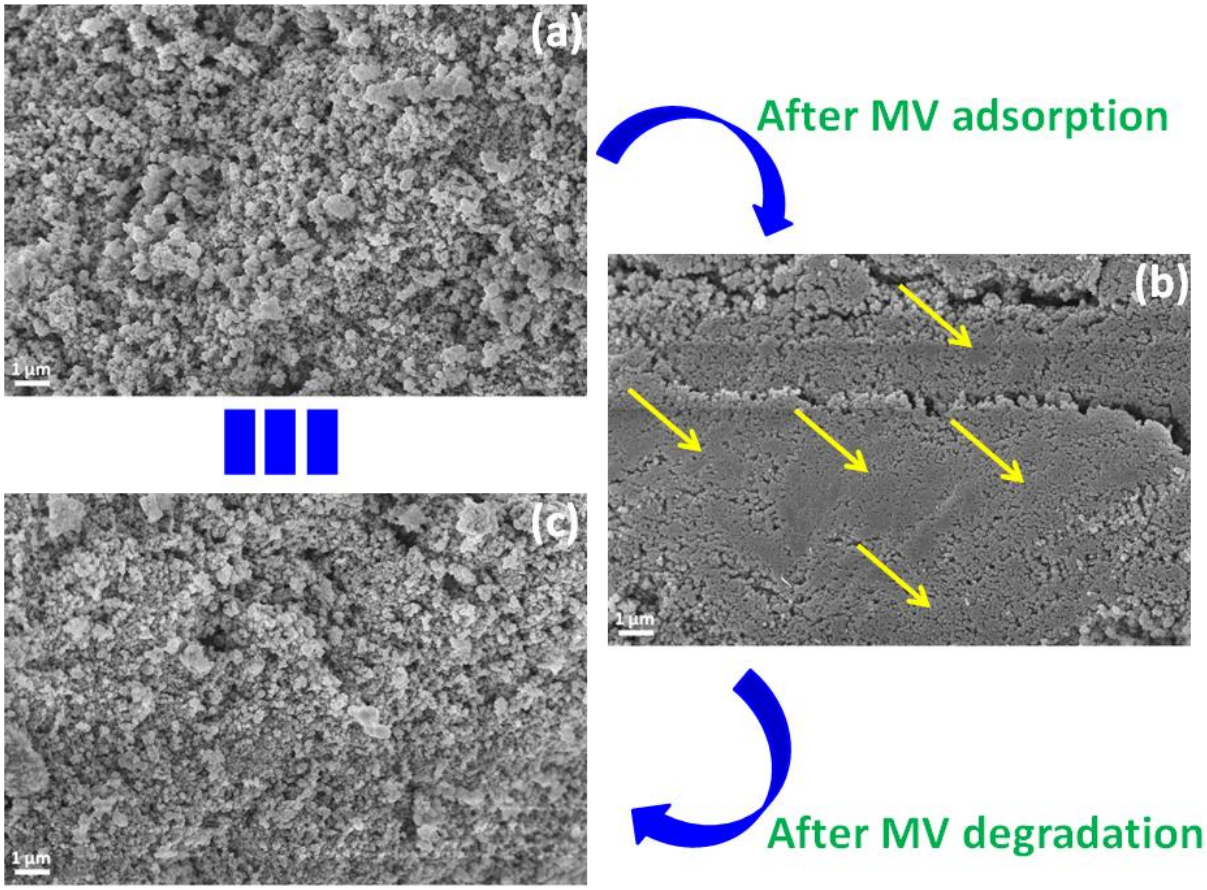

Fig. S25. FE-SEM images of (a) g-AP-pAA/TiO_2-Au nanocomposites (b) MV loaded g-AP-pAA/TiO_2-Au nanocomposites (c) MV degraded g-AP-pAA/TiO_2-Au nanocomposites

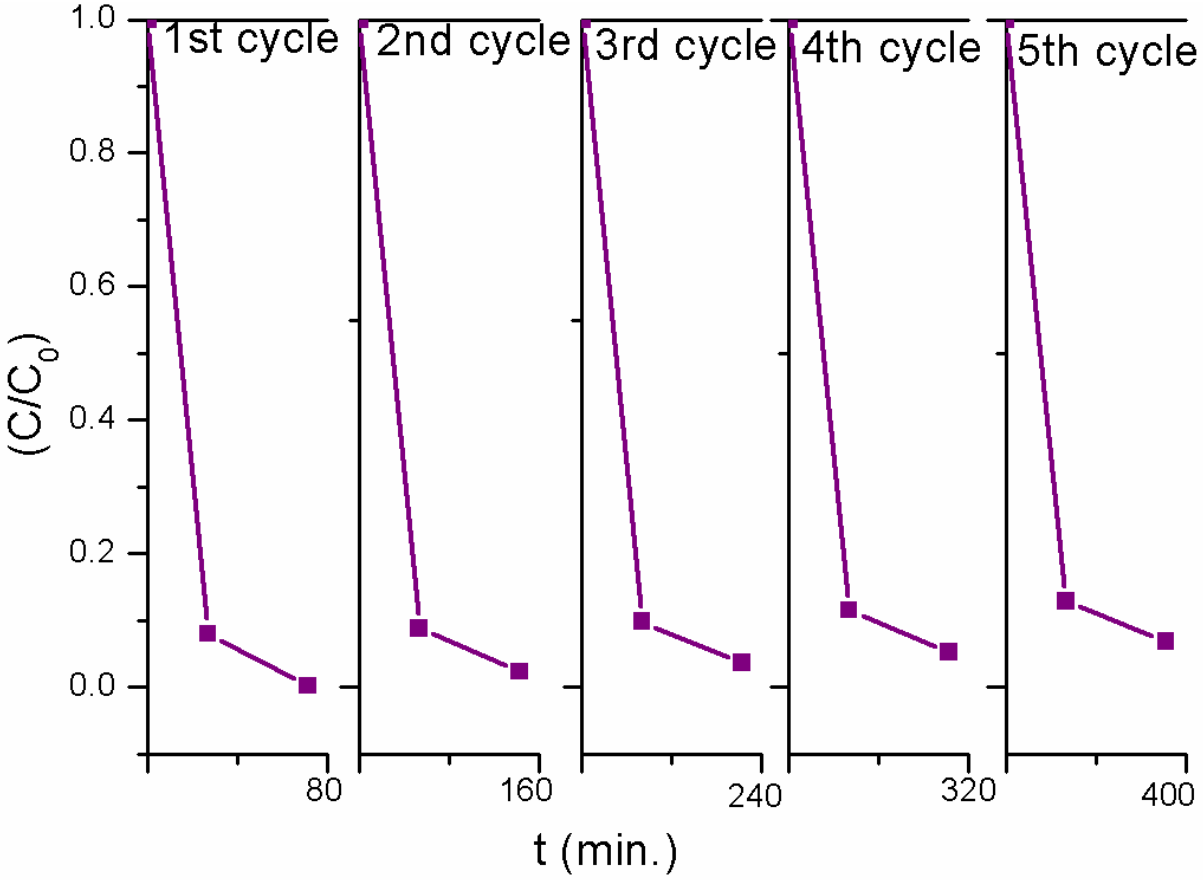

Fig. S26: Consecutive cycles for regeneration study

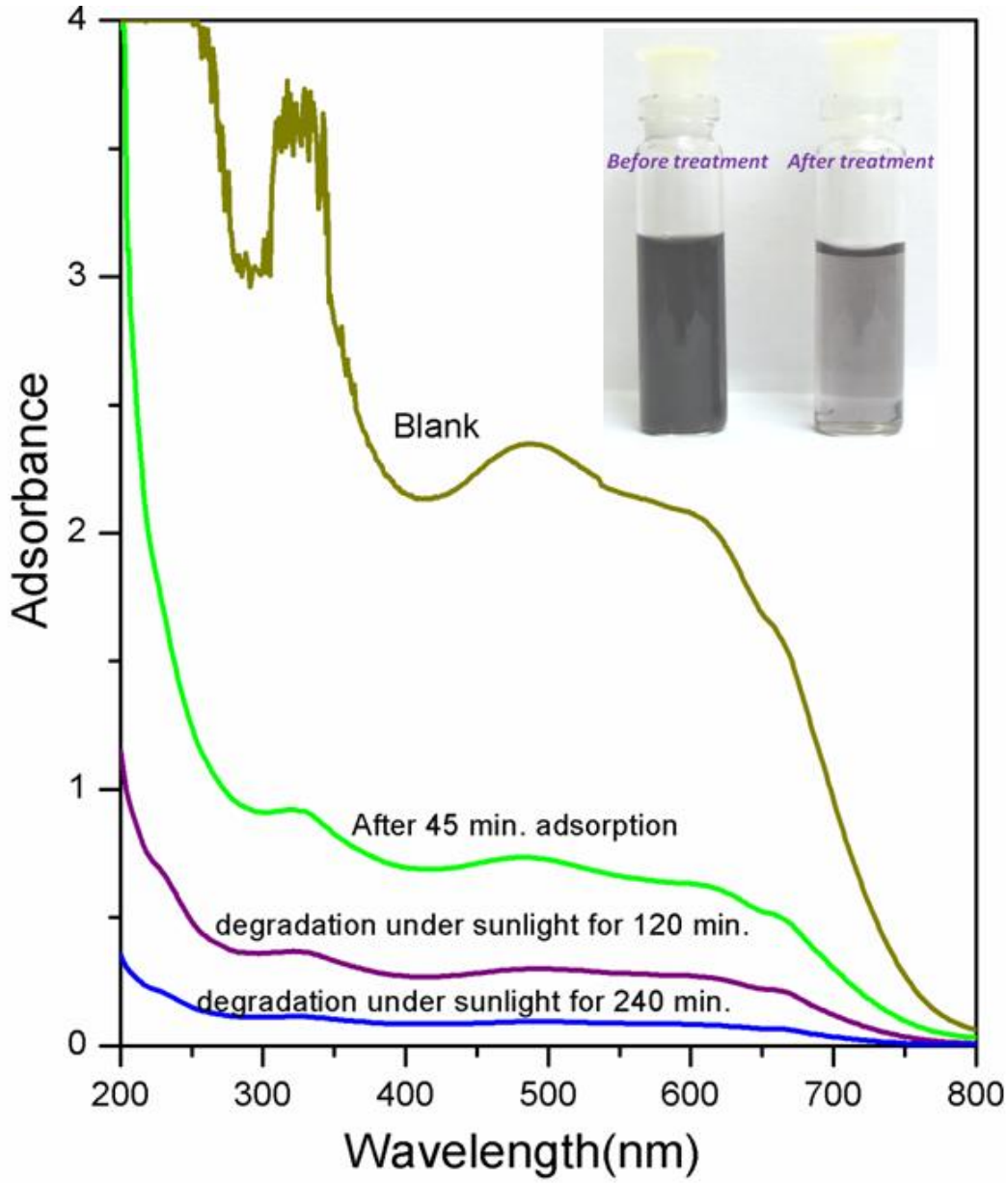

Fig. S27. Treatment of textile effluent by combined effect of adsorption and degradation

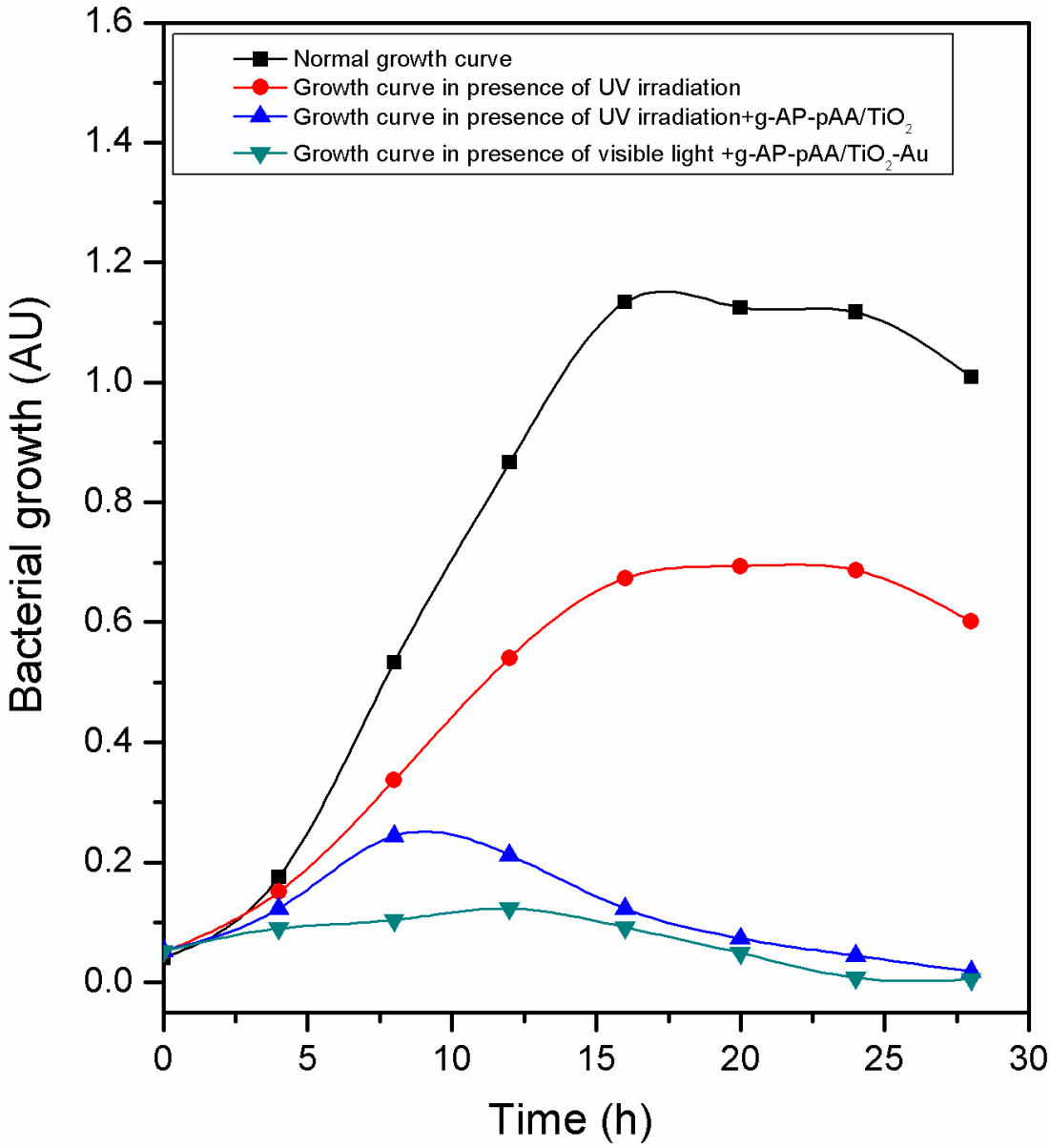

Fig. S28. The bacterial (E. coli) growth curve

Photocatalytic inactivation:

Now, to calculate the difference between the mean specific growth rates of each culture, we first calculated the specific growth rates of collected samples at 4 hours interval. The formula to calculate specific growth rate is as follows.[16]

Specific Growth Rate = $2.303\frac{Log10X_2 - Log10X_1}{T_2 - T_1}$

Where, X_1, X_2 are corresponding bacterial biomass (in terms of Absorption Unit) at time T_1,T_2.

We have calculated the mean Specific Growth Rate and the difference between the control and the test in both cases are significantly high.

SGR Difference:

- Mean SGR of Control in UV– Mean SGR of Test with g-AP-pAA/TiO_2 in UV radiation

  = 0.088822142 – (-0.037895111)

  = 0.126717254

- Mean SGR of Control in visible source – Mean SGR of Test with Compound g-AP-pAA/TiO_2-Au in visible source

  = 0.114418576 – (-0.083650992)

  =0.198069568

The values calculated above is sufficient to declare that g-AP-pAA/TiO_2-Au nanocomposite material have significantly high bactericidal effect than that of the UV activated g-AP-pAA/TiO_2 material.

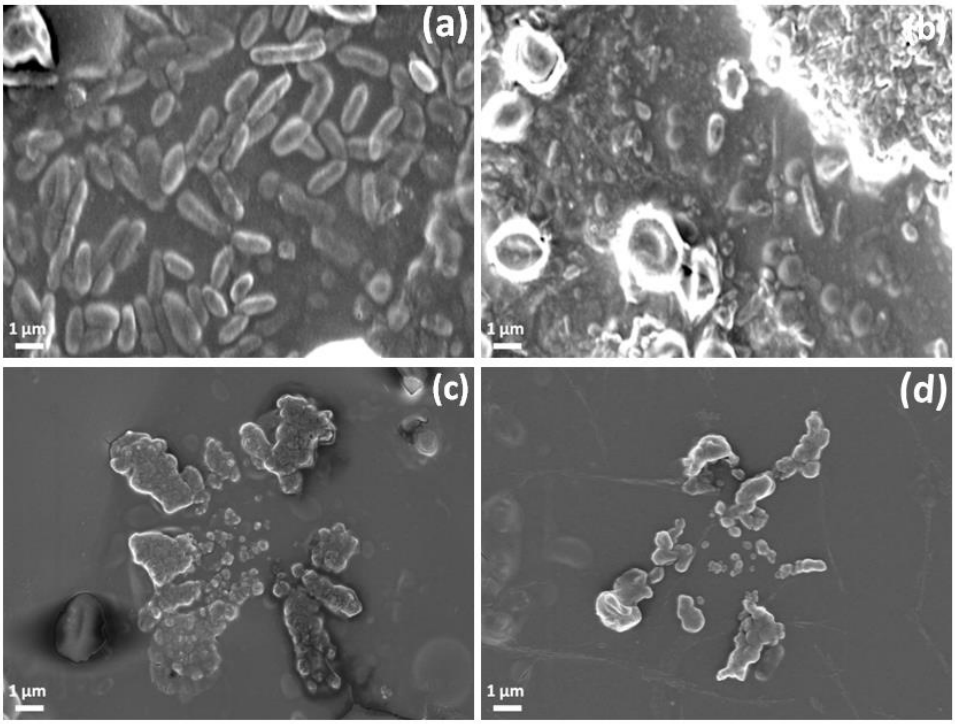

Fig. S29. FESEM images of *E. coli* in (a) absence of light source (b) in presence of UV light source (c) in presence of g-AP-pAA/TiO_2 along with UV light and (d) in presence of g-AP-pAA/TiO_2-Au along with visible light

REFERENCES:

1. Rial, D., Murado, M. A.; Beiras, R.; Vázquez, J. A. Toxicity of Four Spill-Treating Agents on Bacterial Growth and Sea Urchin Embryogenesis. *Chemosphere*, **2014**, *104*, 57-62.

2. Kong, H.; Song, J.; Jang, J. Photocatalytic Antibacterial Capabilities of TiO_2-Biocidal Polymer Nanocomposites Synthesized by a Surface-Initiated Photopolymerization. *Environmental Science & Technology*, **2010**, *44*, 5672-5676.

3. Han, J.; Castell-Perez, M. E.; Moreira, R. G. The Influence of Electron Beam Irradiation of Antimicrobial-Coated LDPE/polyamide Films on Antimicrobial Activity and Film Properties. *LWT - Food Science and Technology*, **2007**, *40*,1545-1554.

4. Legergren, S. About the Theory of So Called Adsorption of Soluble Substances. Kungliga Svenska Vetenskapsakademiens Handlingar., **1898**, *24*, 1-39.

5. Ho, Y.S., McKay, G. Pseudo-Second Order Model for Sorption Processes. *Process Biochemistry*, **1999**, *34*, 451-465.

6. Langmuir, I. The Constitution and Fundamental Properties of Solids and Liquids. *Journal of American Chemical Society*, **1916**, *38*, 2221-2295.

7. Ayad, M. M.; El-Nasr, A. A. Adsorption of Cationic Dye (Methylene Blue) from Water Using Polyaniline Nanotubes Base. *Journal of Physical Chemistry C*, **2010**, *114*, 14377-14383.

8. Freundlich, H. M. F. Uber die Adsorption in Losungen, *Z. Phys. Chem.* **1906**, *57*, 385-470.

9. Cho, E.; Tahir, M. N.; Kim, H.; Yud, J. H.; Jung, Seunho. Removal of Methyl Violet Dye by Adsorption onto N benzyltriazole Derivatized Dextran. *RSC Advances*, **2015**, 5, 34327–34334

10. Dahri, M. K.; Kooh, M.R.R.; Lim, L. B. L. Removal of Methyl Violet 2B from Aqueous Solution Using *Casuarina equisetifolia* Needle. *Hindawi Publishing Corporation ISRN Environmental Chemistry*. **2013**, Article ID 619819.

11. Xu, S.; Wang, J.; Wu, R.; Wang J.; Li, H.; Adsorption Behaviors of Acid and Basic Dyes on Crosslinked Amphoteric Starch. *Chemical Engineering Journal*, **2006,** *117*, 161–167.

12. Ghorai, S.; Sarkar, A.; Raoufi, M.; Panda, A.B.; Schönherr, H.; Pal, S. Enhanced Removal of Methylene Blue and Methyl Violet Dyes from Aqueous Solution Using a Nanocomposite of Hydrolyzed Polyacrylamide Grafted Xanthan Gum and Incorporated Nanosilica. *ACS Applied Materials & Interfaces*, **2014**, *6*, 4766-4777.

13. Liu, R.; Zhang, B.; Mei, D.; Zhang, H.; Liu, J. Adsorption of Methyl Violet from Aqueous Solution by Halloysite Nanotubes. *Desalination* **2011,** *268*, 111–116.

14. Zhou, Li.; Huang, J.; He, B.; Zhang, F.; Li, H. Peach Gum for Efficient Removal of Methylene Blue and Methyl Violet Dyes from Aqueous Solution. *Carbohydrate Polymers*, **2014**, *101*, 574-581.

15. Azizian, S.; Haerifar, M.; Bashiri, H. Adsorption of Methyl Violet onto Granular Activated Carbon: Equilibrium, Kinetics and Modeling. *Chemical Engineering Journal***, 2009,** *146*, 36–41.

16. Widdel, F.Theory and Measurement of Bacterial Growth. *Di Dalam Grundpraktikum Mikrobiologie*, **2007**,1–11.